Signal Processing 92 (2012) 939–953

Contents lists available at SciVerse ScienceDirect

Signal Processing

journal homepage: www.elsevier.com/locate/sigpro

Extended-aperture angle-range estimation of multiple Fresnel-region sources with a linear tripole array using cumulants

Jin He, M. Omair Ahmad *, M.N.S. Swamy

Center for Signal Processing and Communications, Department of Electrical and Computer Engineering, Concordia University, Montréal, QC, Canada H3G 1M8

ARTICLE INFO

Article history:
Received 15 March 2011
Received in revised form
6 July 2011
Accepted 20 September 2011
Available online 25 October 2011

Keywords:
Array signal processing
Fresnel-region
Tripole array
Directions-of-arrival
ESPRIT
Cumulant

ABSTRACT

This paper presents a cumulant-based algorithm to achieve aperture extension for estimating the directions-of-arrival (DOAs) and the ranges of multiple Fresnel-region sources using a linear tripole array. The proposed algorithm defines two cumulant-based matrices, from which the DOA and the range of each source are estimated from the source's tripole steering vector using the ESPRIT technique. These are then used as coarse reference estimates to disambiguate the cyclic phase ambiguities induced from the spatial phase factors when the inter-sensor spacing exceeds a half wavelength. The algorithm does not require two-dimensional searching or parameter pairing, and can resolve $3(L-1)$ sources with L tripoles. The extension of the proposed algorithm by formulating multiple cumulant matrices and using parallel factor (PARAFAC) analysis is also presented. Simulation results are provided demonstrating the significant improvement in the performance over that of several existing algorithms.

1. Introduction

Estimation of the directions-of-arrival (DOAs) using sensor array techniques has received a significant amount of attention over the past decades [1]. Many efficient algorithms, such as MUSIC [2] and ESPRIT [3] and their derivatives, have been developed to deal with this issue. Most of these algorithms assume far-field incoming sources, so that the wavefronts from these sources can be considered as plane waves at the sensor array, and therefore, each source location can be parameterized by a single DOA [1]. However, in many practical applications, such as near-field sonar applications [4], seismic exploration [5], and electronic surveillance [6], this far-field assumption is no longer valid, since the ranges of the sources to the array are not sufficiently large compared with the diameter of the sensor array [7]. In this case, the wavefront emitted by a source is spherical rather than planar at the site of the sensor array, and the source location should be characterized by both the range and the DOA [4–6].

With the near-field restricted to the Fresnel-region [14], many advanced algorithms have been developed to solve the angle-range estimation problem. These algorithms include the maximum likelihood algorithm [8], the two-dimensional MUSIC algorithm [9], the path following algorithm [10] and its modified version [11], the polynomial rooting algorithm [12], the weighted linear prediction algorithm [13], the two-step searching algorithm [14], and the higher-order statistics (HOS) based algorithms [15–21]. However, most of these algorithms involve either two-dimensional searching or parameter pairing. Moreover, all of the above mentioned algorithms require inter-sensor spacing within a quarter or a half wavelength to guarantee unique and unambiguous angle and range estimates.

It is well known that an array with larger aperture can offer higher array resolution and more accurate parameter estimation precision. Extending the array aperture by adding

* Corresponding author. Tel.: +1 514 848 2424; fax: +1 514 848 2808.
E-mail address: omair@ece.concordia.ca (M. Omair Ahmad).

0165-1684/$ - see front matter © 2011 Elsevier B.V. All rights reserved.
doi:10.1016/j.sigpro.2011.09.037

more sensors would increase the hardware costs and would add to the computational load required by the signal processors. Extending the array aperture by extending the uniform inter-sensor spacing beyond a half-wavelength will lead to a set of cyclically ambiguous angle/range estimates, in accordance with the spatial Nyquist theorem. It is worth mentioning that for far-field parameter estimation, unambiguous and accurate parameter estimates can be achieved by deploying special sensors that measure the vector components of the impinging electromagnetic vector-field [22] or of the underwater acoustic vector-field [23], or by having a sparse array grid geometry that may embed two or more widths of spatial invariance [24,25], or by adopting higher order statistics to construct "virtual sensors" [26,27]. Motivated by the fact that array aperture extension (without adding more sensors) has been achieved for improving the estimation of far-field signal parameters, it is of practical importance to investigate the problem of extended aperture for improving the estimation of Fresnel-region signal parameters. In fact, it should be mentioned that for large aperture arrays, sources are often located in the Fresnel-region. We present a cumulant-based algorithm to estimate the directions-of-arrival (DOAs) and the ranges of multiple Fresnel-region sources using sparse linear tripoles, each of which consists of three spatially co-located antennas measuring the three electrical-field components of the incident wavefield. The proposed algorithm defines two cumulant-based matrices, from which the DOA and the range of each source are estimated from the source's tripole steering vector by using the ESPRIT technique. These DOA and range estimates are then used as coarse reference estimates to disambiguate the cyclic phase ambiguities induced from the spatial phase factors when the inter-sensor spacing exceeds a half wavelength. Compared with most of the existing algorithms, the proposed algorithm requires neither two-dimensional searching nor parameter pairing, and can resolve $3(L-1)$ sources with L tripoles. The extension of the proposed algorithm by formulating multiple cumulant matrices and using parallel factor (PARAFAC) analysis is also presented. Moreover, the Cramér–Rao bound (CRB) for the problem under consideration is derived to evaluate the performance of the proposed algorithms. It should be noted that the present algorithm is related to the algorithms in [19,22,28] in the sense that the basic step (using coarse estimates to resolve ambiguous estimates) of the present algorithm is the same as that in [22], and the cumulant-based matrices defined in the present algorithm are in a way similar to those defined in [19,28]. Also, the present algorithm can be considered as a generalization of the closely spaced cross-dipole in [19] to the case of sparse tripole array. However, since the sensors used in the present algorithm are different from those in [19,22,28], the derivation of the algorithm and its performance bounds are different from those in [19,22,28]. For example, (i) [22] deals with the far-field signals, whereas the present algorithm deals with the Fresnel-region signals, (ii) the coarse parameter estimates in the algorithm in [22] are obtained via vector cross product, whereas in the proposed algorithm, they are estimated by solving nonlinear equations, and (iii) the algorithms in [19] and [28] cannot be applied to the sparse sensor array, such as the one considered in the proposed algorithm.

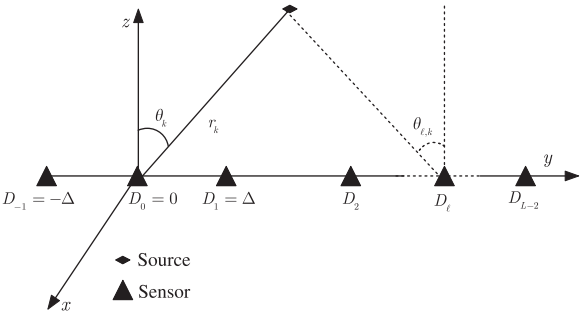

Fig. 1. Array configuration for the proposed algorithm.

The paper is organized as follows. Section 2 gives the mathematical data model of Fresnel-region source localization with a sparse linear tripole array and the problem formulation. Section 3 develops the extended aperture angle-range estimation algorithm. Section 4 presents the extension of the proposed algorithm by formulating multiple cumulant matrices and using parallel factor (PARAFAC) analysis. Section 5 provides the simulation results demonstrating the efficacy of the proposed algorithm. Section 6 concludes the paper.

2. Data model and problem formulation

The present signal model involves K Fresnel-region uncorrelated non-Gaussian transverse electromagnetic waves, traveling through a homogeneous isotropic medium, and impinging upon an L-element sparse linear tripole array, as shown in Fig. 1. We assume all the sensors $(-1,0,1,\ldots,L-2)$ to lie on the y-axis with locations $D_{-1}=-\Delta$, $D_0=0$, $D_1=\Delta$, $D_2,\ldots,D_{L-2}$, relative to the origin. The spacing Δ in this paper is assumed to exceed a half-wavelength. Further, for simplicity, we assume that the impinging signals are in the y–z plane.[1] Then, the incoming signals can be parameterized by $(\theta_k,\gamma_k,\eta_k,r_k)$, $k=1,\ldots,K$, where $\theta_k\in[0,\pi/2]$ and r_k respectively denote the DOA and the range of the kth source at the reference sensor 0, $\gamma_k\in[0,\pi/2)$ and $\eta_k\in[-\pi,\pi)$ are, respectively, the auxiliary polarization angle and the polarization phase difference of the kth source. Let $\mathbf{e}_{\ell,k}$ be the electric field vector of the kth unit-power completely polarized electromagnetic wavefront at the ℓ th tripole; then, $\mathbf{e}_{\ell,k}$ can be expressed as[2] [29,30]

$$\begin{aligned}\mathbf{e}_{\ell,k}&=[\vec{\mathbf{v}}_\phi,\vec{\mathbf{v}}_\theta]\mathbf{g}(\gamma_k,\eta_k)\\&=\mathrm{diag}(\vec{\mathbf{v}}_x,\vec{\mathbf{v}}_y,\vec{\mathbf{v}}_z)\begin{bmatrix}0&-1\\\cos\theta_{\ell,k}&0\\-\sin\theta_{\ell,k}&0\end{bmatrix}\mathbf{g}(\gamma_k,\eta_k)\\&=-\cos\gamma_k\vec{\mathbf{v}}_x+\sin\gamma_k\cos\theta_{\ell,k}e^{j\eta_k}\vec{\mathbf{v}}_y-\sin\gamma_k\sin\theta_{\ell,k}e^{j\eta_k}\vec{\mathbf{v}}_z\end{aligned}\tag{1}$$

[1] Note that the azimuth angles (ϕ) of incoming signals become $\pi/2$ in this scenario, so that only the elevation angles and ranges need to be estimated. However, the present algorithm can be easily extended to the estimation of the joint azimuth-elevation angles and ranges by placing an additional array along the x-axis.

[2] The detailed derivation of this equation can be found in [29].

where $\vec{\mathbf{v}}_\phi$, $\vec{\mathbf{v}}_\theta$ are, respectively, the unit vectors along the subscript's coordinate, $\vec{\mathbf{v}}_x$,$\vec{\mathbf{v}}_y$, and $\vec{\mathbf{v}}_z$ are, respectively, the unit vectors along the x, y, and z-axes, $\mathbf{g}(\gamma_k,\eta_k) = [\sin\gamma_k e^{j\eta_k}, \cos\gamma_k]^T$ is the polarization vector of the signal, and $\theta_{\ell,k}$ is the DOA of the kth source at the ℓ th tripole. The DOA $\theta_{\ell,k}$ is related to θ_k as [17,19]

$$\theta_{\ell,k} = \arcsin\left(\frac{r_k \sin\theta_k - D_\ell}{\sqrt{r_k^2 + D_\ell^2 - 2r_k D_\ell \sin\theta_k}}\right) \tag{2}$$

and $\theta_{\ell,k} = \theta_k$, for $\ell = 0$. Eq. (2) indicates that the value of incident angle varies at each of the L tripoles, this property is pivotal in deriving coarse reference range estimates of the incoming signals. Expressed in matrix form, the ℓ th tripole's steering vector of the kth signal would produce the following 3×1 vector[3]

$$\mathbf{e}_{\ell,k} = \begin{bmatrix} e_1(\theta_{\ell,k},\gamma_k,\eta_k,r_k) \\ e_2(\theta_{\ell,k},\gamma_k,\eta_k,r_k) \\ e_3(\theta_{\ell,k},\gamma_k,\eta_k,r_k) \end{bmatrix} = \begin{bmatrix} -\cos\gamma_k \\ \sin\gamma_k \cos\theta_{\ell,k} e^{j\eta_k} \\ -\sin\gamma_k \sin\theta_{\ell,k} e^{j\eta_k} \end{bmatrix} \tag{3}$$

The delay $\tau_{\ell,k}$ associated with the kth source signal propagation time between the tripoles located at D_0 and D_ℓ is of the form[4]

$$\tau_{\ell,k} = \frac{2\pi}{\lambda}\left(\sqrt{r_k^2 + D_\ell^2 - 2r_k D_\ell \sin\theta_k} - r_k\right) \tag{4}$$

where λ denotes the wavelength of the source wavefronts. This is a nonlinear function of the parameters θ_k and r_k, and consequently, the conventional high-resolution angle estimation methods cannot be applied to extract the parameters θ_k and r_k directly. However, when the signal is in the Fresnel-region, $\tau_{\ell,k}$ can be approximated by using the second-order Taylor expansion

$$\tau_{\ell,k} \approx -\frac{2\pi}{\lambda} D_\ell \sin\theta_k + \frac{\pi}{\lambda r_k} D_\ell^2 \cos^2\theta_k + O\left(\frac{D_\ell^2}{r_k^2}\right) \tag{5}$$

where $O(D_\ell^2/r_k^2)$ represents terms of order greater than or equal to D_ℓ^2/r_k^2, and these terms are neglected here. Using this approximation, the inter-sensor spatial phase factor related to the kth signal and the ℓ th dipole is

$$q_\ell(\theta_k,r_k) = e^{j(-(2\pi/\lambda)D_\ell \sin\theta_k + (\pi/(\lambda r_k))D_\ell^2 \cos^2\theta_k)} \tag{6}$$

The $3L\times 1$ array manifold for the entire L-element tripole array is

$$\mathbf{a}(\theta_k,\gamma_k,\eta_k,r_k) = \begin{bmatrix} q_{-1}(\theta_k,r_k)\mathbf{e}_{-1,k} \\ \mathbf{e}_{0,k} \\ q_1(\theta_k,r_k)\mathbf{e}_{1,k} \\ \vdots \\ q_{L-2}(\theta_k,r_k)\mathbf{e}_{L-2,k} \end{bmatrix} \tag{7}$$

The vector $\mathbf{q}(\theta_k,r_k) \triangleq [q_{-1}(\theta_k,r_k),1,q_1(\theta_k,r_k),\ldots,q_{L-2}(\theta_k,r_k)]^T$ denotes the steering vector corresponding to the signal parameters (θ_k,r_k) of a scalar sensor array that has the same array geometry as the tripole array geometry in Fig. 1.

With a total of K signals, the entire array would yield $3L\times 1$ vector measurements $\mathbf{z}(t)$ at time t

$$\mathbf{z}(t) = \sum_{k=1}^{K} \mathbf{a}(\theta_k,\gamma_k,\eta_k,r_k)s_k(t) + \mathbf{n}(t) = \mathbf{A}\mathbf{s}(t) + \mathbf{n}(t) \tag{8}$$

where $s_k(t)$ stands for the phasor representation of the kth signal, $\mathbf{s}(t) = [s_1(t),\ldots,s_K(t)]^T$ denotes the signal vector, $\mathbf{A} = [\mathbf{a}(\theta_1,\gamma_1,\eta_1,r_1),\ldots,\mathbf{a}(\theta_K,\gamma_K,\eta_K,r_K)]$ is the $3L\times K$ array manifold matrix, and $\mathbf{n}(t)$ represents the $3L\times 1$ additive noise vector. From (8), the element $z_{\ell,m}(t)$, which denotes the data measured by the mth ($m = 1,2,3$) element of the ℓ th tripole, can be expressed as

$$z_{\ell,m}(t) = \sum_{k=1}^{K} e_m(\theta_{\ell,k},\gamma_k,\eta_k,r_k)q_\ell(\theta_k,r_k)s_k(t) + n_{\ell,m}(t) \tag{9}$$

With a total of N snapshots taken at the distinct instants $\{t_n : n = 1,\ldots,N\}$, the problem is to determine the angle and range parameters $\{\theta_k,r_k,k = 1,\ldots,K\}$ of the impinging signals from these snapshots. For beamforming purposes, it may be also useful to estimate the corresponding polarization parameters $\{\gamma_k,\eta_k,k = 1,\ldots,K\}$. We provide a solution to the above-mentioned problems in Section 3, under the following assumptions.

(i) The signal parameters $(\theta_1,\gamma_1,\eta_1,r_1),\ldots,(\theta_K,\gamma_K,\eta_K,r_K)$ are pairwise distinct.
(ii) The impinging signals are zero-mean and stationary, mutually independent, and non-Gaussian, having nonzero fourth-order cumulants.
(iii) The noise is zero-mean, complex Gaussian, and possibly spatially correlated.
(iv) The noise is statistically independent of all the signals.

3. The proposed extended-aperture angle-range estimation

3.1. Formulation of the cumulant matrices

For the Fresnel-region scenario, the basic ESPRIT (second-order statistics based) algorithm cannot be applied to the measured data directly. In this subsection, by applying the higher-order statistics, we formulate two cumulant matrices to enable us the application of the ESPRIT idea to recover the angle and range parameters of the incoming signals. The fourth-order cumulant of $z_{i,m}(t)$, $z_{j,m}(t)$, $z_{p,m}(t)$,

[3] For signals located in a 3D space, the ℓ th tripole's steering vector of the kth signal would produce the following 3×1 vector:

$$\mathbf{e}_{\ell,k} = \begin{bmatrix} e_1(\theta_{\ell,k},\phi_{\ell,k},\gamma_k,\eta_k,r_k) \\ e_2(\theta_{\ell,k},\phi_{\ell,k},\gamma_k,\eta_k,r_k) \\ e_3(\theta_{\ell,k},\phi_{\ell,k},\gamma_k,\eta_k,r_k) \end{bmatrix} = \begin{bmatrix} \sin\gamma_k \cos\theta_{\ell,k}\cos\phi_{\ell,k}e^{j\eta_k} - \cos\gamma_k \sin\phi_{\ell,k} \\ \sin\gamma_k \cos\theta_{\ell,k}\sin\phi_{\ell,k}e^{j\eta_k} + \cos\gamma_k \cos\phi_{\ell,k} \\ -\sin\gamma_k \sin\theta_{\ell,k}e^{j\eta_k} \end{bmatrix}$$

For signals located in $y-z$ plane, this equation reduces to (3).

[4] For a planar array in the $x-y$ plane, the delay $\tau_{\ell,k}$ associated with the kth source signal propagation time between the tripoles located at D_0 and D_{ℓ_x,ℓ_y} is of the form

$$\tau_{\ell,k} = \frac{2\pi}{\lambda}\left(\sqrt{(r_k \sin\theta_k \cos\phi_k - D_{\ell_x})^2 + (r_k \sin\theta_k \sin\phi_k - D_{\ell_y})^2 + (r_k \cos\theta_k)^2} - r_k\right)$$

For the case when the impinging signals are in the $y-z$ plane and the tripoles are located along the y-axis, this equation simplifies to (4).

$z_{l,m}(t)$ is given by [31]

$$\begin{aligned}\mathrm{cum}(z_{i,m}(t),z^*_{j,m}(t),z_{p,m}(t),z^*_{l,m}(t)) &= E\{z_{i,m}(t)z^*_{j,m}(t)z_{p,m}(t)z^*_{l,m}(t)\}\\ &-E\{z_{i,m}(t)z^*_{j,m}(t)\}E\{z_{p,m}(t)z^*_{l,m}(t)\}\\ &-E\{z_{i,m}(t)z^*_{l,m}(t)\}E\{z_{p,m}(t)z^*_{j,m}(t)\}\\ &-E\{z_{i,m}(t)z_{p,m}(t)\}E\{z^*_{l,m}(t)z^*_{j,m}(t)\}\end{aligned} \tag{10}$$

Then, we define the following two cumulant-based matrices

$$\mathbf{R}_1 = \sum_{m=1}^{3} \mathrm{cum}(z_{0,m}(t),z^*_{0,m}(t),\mathbf{z}(t),\mathbf{z}^H(t)) \tag{11}$$

$$\mathbf{R}_2 = \sum_{m=1}^{3} \mathrm{cum}(z_{-1,m}(t),z^*_{1,m}(t),\mathbf{z}(t),\mathbf{z}^H(t)) \tag{12}$$

We prove in Appendix A that the matrices $\mathbf{R}_1$ and $\mathbf{R}_2$ have the form

$$\mathbf{R}_1 = \mathbf{A}\boldsymbol{\Gamma}\mathbf{A}^H \tag{13}$$

and

$$\mathbf{R}_2 = \mathbf{A}\boldsymbol{\Phi}\boldsymbol{\Gamma}\mathbf{A}^H \tag{14}$$

where

$$\boldsymbol{\Gamma} = \mathrm{diag}\left\{\zeta_1 \sum_{m=1}^{3} |e_m(\theta_1,\phi_1,\gamma_1,r_1)|^2,\ldots,\zeta_K \sum_{m=1}^{3} |e_m(\theta_K,\phi_K,\gamma_K,r_K)|^2\right\} \tag{15}$$

$$\boldsymbol{\Phi} = \mathrm{diag}\left\{\beta_1 e^{j(4\pi/\lambda)\Delta \sin\theta_1},\ldots,\beta_K e^{j(4\pi/\lambda)\Delta \sin\theta_K}\right\} \tag{16}$$

In (15) and (16)

$$\zeta_k = \mathrm{cum}(s_k(t),s^*_k(t),s_k(t),s^*_k(t)) \tag{17}$$

is the kurtosis of the kth signal, and

$$\beta_k = \frac{\sum_{m=1}^{3} e_m(\theta_{-1,k},\gamma_k,\eta_k,r_k)e^*_m(\theta_{1,k},\gamma_k,\eta_k,r_k)}{\sum_{m=1}^{3} |e_m(\theta_k,\gamma_k,\eta_k,r_k)|^2} \tag{18}$$

is a real-valued parameter that is related to the signal parameters. In computing the matrices $\mathbf{R}_1$ and $\mathbf{R}_2$, we take the sum over the number of components of the tripole in order to preserve the signal power and to enhance noise cancelation.

From (13) and (14), we see that the matrix pencil $\{\mathbf{A},\mathbf{A}\boldsymbol{\Phi}\}$ has generalized eigenvalues related to the angles of the signals, and forms the diagonal entries of $\boldsymbol{\Phi}$. Therefore, application of ESPRIT to the matrix pencil $\{\mathbf{A},\mathbf{A}\boldsymbol{\Phi}\}$ would yield a set of angle estimates, as well as a set of array steering vector estimates.

3.2. Low-variance but cyclically ambiguous angle estimates

Under the assumptions made in the previous section, the matrices $\mathbf{A}$ and $\boldsymbol{\Gamma}$ are of full rank. Then, using the basic idea of ESPRIT [3], the $6L \times K$ signal subspace matrix $\mathbf{E}_s$ of $\mathbf{R} = [\mathbf{R}_1^T,\mathbf{R}_2^T]^T$ can be expressed as

$$\mathbf{E}_s = \begin{bmatrix}\mathbf{A}\\ \mathbf{A}\boldsymbol{\Phi}\end{bmatrix}\mathbf{T} \tag{19}$$

where $\mathbf{E}_s$ is composed of the K vectors corresponding to the K largest singular values of $\mathbf{R}$, and $\mathbf{T}$ denotes an unknown $K \times K$ nonsingular matrix to be determined. Defining $\mathbf{E}_1$ to be the first $3L$ rows of $\mathbf{E}_s$ and $\mathbf{E}_2$ to be the last $3L$ rows of $\mathbf{E}_s$, we have

$$\mathbf{E}_1 = [\mathbf{I}_{3L} \vdots \mathbf{O}_{3L}]\mathbf{E}_s = \mathbf{A}\mathbf{T} \tag{20}$$

$$\mathbf{E}_2 = [\mathbf{O}_{3L} \vdots \mathbf{I}_{3L}]\mathbf{E}_s = \mathbf{A}\boldsymbol{\Phi}\mathbf{T} \tag{21}$$

where $\mathbf{I}_i$ signifies the $i \times i$ identity matrix, and $\mathbf{O}_i$ denotes an $i \times i$ matrix whose elements are all zeroes. Eqs. (20) and (21) together imply that there exists a $K \times K$ nonsingular matrix $\boldsymbol{\Psi}$ relating the two $3L \times K$ full rank matrices $\mathbf{E}_1$ and $\mathbf{E}_2$ as

$$\mathbf{E}_1\boldsymbol{\Psi} = \mathbf{E}_2 \Rightarrow \mathbf{A}\mathbf{T}\boldsymbol{\Psi} = \mathbf{A}\boldsymbol{\Phi}\mathbf{T} \tag{22}$$

$$\Rightarrow \boldsymbol{\Psi} = \mathbf{E}_1^{\dagger}\mathbf{E}_2 = \mathbf{T}^{-1}\boldsymbol{\Phi}\mathbf{T} \tag{23}$$

where the superscript † denotes the pseudo inverse.

Eq. (23) indicates that the diagonal elements $\{\Phi_{k,k} = \beta_k e^{j(4\pi/\lambda)\Delta \sin\theta_k},\ k = 1,\ldots,K\}$ constitute the eigenvalues of $\boldsymbol{\Psi}$. Since $\Delta > \lambda/2$ and $|\sin\theta_k| \le 1$, there exists a set of cyclically ambiguous estimates of θ_k that satisfy (23). These estimates of θ_k are computed as

$$\begin{aligned}&\hat{\theta}_k(n_\theta) = \arcsin\left(\vartheta_k + n_\theta\frac{\lambda}{2\Delta}\right)\\ &\left\lceil\frac{2\Delta}{\lambda}(-1-\vartheta_k)\right\rceil \le n_\theta \le \left\lfloor\frac{2\Delta}{\lambda}(1-\vartheta_k)\right\rfloor\\ &\vartheta_k = \frac{\angle\{[\boldsymbol{\Phi}]_{k,k}\}}{4\pi\Delta/\lambda},\quad k = 1,\ldots,K\end{aligned} \tag{24}$$

where n_θ is an integer, $\lceil x\rceil$ denotes the smallest integer not less than x, $\lfloor x\rfloor$ represents the largest integer not greater than x, and $\angle\{z\}$ signifies the principal argument of the complex number z between $-\pi$ and π.

3.3. Unambiguous coarse reference angle estimates

To derive a set of high-variance but unambiguous angle estimates, the tripole array manifolds for each of the K sources, i.e., $\{\mathbf{e}_{0,k}, k = 1,\ldots,K\}$ need to be estimated. This can be accomplished by extracting the fourth to the sixth rows of $\hat{\mathbf{A}}$, which can be estimated by using (20) and (21) as

$$\hat{\mathbf{A}} = [\hat{\mathbf{a}}_1,\ldots,\hat{\mathbf{a}}_K] = \mathbf{E}_1\mathbf{T}^{-1} = \mathbf{E}_2\mathbf{T}^{-1}\boldsymbol{\Phi}^{-1} = \tfrac{1}{2}\{\mathbf{E}_1\mathbf{T}^{-1} + \mathbf{E}_2\mathbf{T}^{-1}\boldsymbol{\Phi}^{-1}\} \tag{25}$$

It should be pointed out that in order to ensure the essential uniqueness for the estimation of $\hat{\mathbf{A}}$, the eigenvalues of the matrix pencil $\{\mathbf{A},\mathbf{A}\boldsymbol{\Phi}\}$ are required to be different. This is guaranteed since $(\theta_k,\gamma_k,\eta_k,r_k) \ne (\theta_\ell,\gamma_\ell,\eta_\ell,r_\ell)$, and hence the eigenvalues $\boldsymbol{\Phi}_{k,k} = \beta_k e^{j4\pi/\lambda\Delta \sin\theta_k} \ne \beta_\ell e^{j4\pi/\lambda\Delta \sin\theta_\ell} = \boldsymbol{\Phi}_{\ell,\ell}$, for all $k \ne \ell$.

We stress that the estimated tripole steering vector $\hat{\mathbf{e}}_{0,k}$ would suffer the *unknown scaling ambiguity*; that is, $\hat{\mathbf{e}}_{0,k} = c\mathbf{e}_{0,k}$, where c is an unknown complex constant. However, this scaling ambiguity can be easily resolved by taking one of the tripole elements as a reference and normalizing the estimated tripole steering vector with respect to it. Also, note that the Frobenius-norm of the tripole steering vector is independent of the parameters of the signal and is equal to unity [32], i.e., $\|\mathbf{e}_{0,k}\| = 1$ for all $(\theta_k,\gamma_k,\eta_k)$. Therefore, the real and imaginary parts of the

normalized estimate $\hat{\mathbf{e}}_{0,k}/\|\hat{\mathbf{e}}_{0,k}\|$ of the tripole steering vector produce the following separable real-valued nonlinear equations:

$$\cos\gamma_k\cos\eta_k=\Re\{[\hat{\mathbf{e}}_{0,k}]_1e^{-j\angle[\hat{\mathbf{e}}_{0,k}]_3}/\|\hat{\mathbf{e}}_{0,k}\|\} \tag{26}$$

$$-\cos\theta_k\sin\gamma_k=\Re\{[\hat{\mathbf{e}}_{0,k}]_2e^{-j\angle[\hat{\mathbf{e}}_{0,k}]_3}/\|\hat{\mathbf{e}}_{0,k}\|\} \tag{27}$$

$$\sin\theta_k\sin\gamma_k=\Re\{[\hat{\mathbf{e}}_{0,k}]_3e^{-j\angle[\hat{\mathbf{e}}_{0,k}]_3}/\|\hat{\mathbf{e}}_{0,k}\|\} \tag{28}$$

$$-\cos\gamma_k\sin\eta_k=\Im\{[\hat{\mathbf{e}}_{0,k}]_1e^{-j\angle[\hat{\mathbf{e}}_{0,k}]_3}/\|\hat{\mathbf{e}}_{0,k}\|\} \tag{29}$$

where the indexes 1, 2, 3 symbolize the first, the second and the third elements of the vector inside the square brackets, and $\Re$ and $\Im$, respectively, represent the real and imaginary parts. Therefore, the coarse reference estimate of θ can be estimated by using (27) and (28) as

$$\hat{\theta}_k^{\mathrm{ref}}=\arctan\left|\frac{\Re\{[\hat{\mathbf{e}}_{0,k}]_3e^{-j\angle[\hat{\mathbf{e}}_{0,k}]_3}/\|\hat{\mathbf{e}}_{0,k}\|\}}{\Re\{[\hat{\mathbf{e}}_{0,k}]_2e^{-j\angle[\hat{\mathbf{e}}_{0,k}]_3}/\|\hat{\mathbf{e}}_{0,k}\|\}}\right| \tag{30}$$

In addition, the polarization parameters γ_k and η_k can be estimated as

$$\hat{\gamma}_k=\arcsin\left|\frac{\Re\{[\hat{\mathbf{e}}_{0,k}]_3e^{-j\angle[\hat{\mathbf{e}}_{0,k}]_3}/\|\hat{\mathbf{e}}_{0,k}\|\}+\Re\{[\hat{\mathbf{e}}_{0,k}]_2e^{-j\angle[\hat{\mathbf{e}}_{0,k}]_3}/\|\hat{\mathbf{e}}_{0,k}\|\}}{\sin\hat{\theta}_k^{\mathrm{ref}}-\cos\hat{\theta}_k^{\mathrm{ref}}}\right| \tag{31}$$

$$\hat{\eta}_k=-\angle\{[\hat{\mathbf{e}}_{0,k}]_1e^{-j\angle[\hat{\mathbf{e}}_{0,k}]_3}\} \tag{32}$$

The estimation $\hat{\gamma}_k$ and $\hat{\eta}_k$ will be subsequently used to compute cyclically ambiguous range estimates.

3.4. Unambiguous and cyclically ambiguous range estimates

To derive the unambiguous range estimates, we need to extract the array manifold of the tripole $\ell=-1$ for each of the K sources, i.e., $\{\mathbf{e}_{-1,k},k=1,\ldots,K\}$; these can be obtained by normalizing each column of the first to the third rows of $\hat{\mathbf{A}}$. Next, following the same procedure as in the previous subsection, we can get the estimates $\hat{\theta}_{-1,k}$ as

$$\hat{\theta}_{-1,k}=\arctan\left|\frac{\Re\{[\hat{\mathbf{e}}_{-1,k}]_3e^{-j\angle[\hat{\mathbf{e}}_{-1,k}]_3}/\|\hat{\mathbf{e}}_{-1,k}\|\}}{\Re\{[\hat{\mathbf{e}}_{-1,k}]_2e^{-j\angle[\hat{\mathbf{e}}_{-1,k}]_3}/\|\hat{\mathbf{e}}_{-1,k}\|\}}\right| \tag{33}$$

Finally, with the estimation of $\hat{\theta}_{-1,k}$ and $\hat{\theta}_k^{\mathrm{ref}}$ and using the relationship (2), the reference range estimates r_k^{ref} can be obtained by solving the equation

$$(\sin^2\hat{\theta}_{-1,k}-\sin^2\hat{\theta}_k^{\mathrm{ref}})r_k^2+2D_{-1}\sin\hat{\theta}_k^{\mathrm{ref}}\cos^2\hat{\theta}_{-1,k}r_k-D_{-1}^2\cos^2\hat{\theta}_{-1,k}=0 \tag{34}$$

Manipulation of this equation gives[5]

$$\hat{r}_k^{\mathrm{ref}}=\frac{\cos\hat{\theta}_{-1,k}(\sin\hat{\theta}_k^{\mathrm{ref}}\cos\hat{\theta}_{-1,k}+\sin\hat{\theta}_{-1,k}\cos\hat{\theta}_k^{\mathrm{ref}})}{\sin^2\hat{\theta}_{-1,k}-\sin^2\hat{\theta}_k^{\mathrm{ref}}}\Delta \tag{36}$$

[5] For Eq. (34), there is another solution, namely

$$\hat{r}_k^{\mathrm{ref}}=\frac{\cos\hat{\theta}_{-1,k}(\sin\hat{\theta}_k^{\mathrm{ref}}\cos\hat{\theta}_{-1,k}-\sin\hat{\theta}_{-1,k}\cos\hat{\theta}_k^{\mathrm{ref}})}{\sin^2\hat{\theta}_{-1,k}-\sin^2\hat{\theta}_k^{\mathrm{ref}}}\Delta \tag{35}$$

The cyclically ambiguous range estimates can also be found from the spatial phase difference between the tripole $\ell=-1$ and the tripole $\ell=0$. Referring to (7) and (25), aside from the unknown scaling ambiguity, the kth column of first three rows of $\hat{\mathbf{A}}$ would give the estimate $\hat{\mathbf{a}}_{-1}(\theta_k,\gamma_k,\eta_k,r_k)=\hat{\mathbf{e}}_{-1,k}\hat{q}_{-1}(\theta_k,r_k)$, and the kth column of fourth to the sixth rows of $\hat{\mathbf{A}}$ would give the estimate $\hat{\mathbf{a}}_0(\theta_k,\gamma_k,\eta_k,r_k)=\hat{\mathbf{e}}_{0,k}\hat{q}_0(\theta_k,r_k)$. With the estimates $\hat{\theta}_{-1,k}$, $\hat{\theta}_k^{\mathrm{ref}}$, $\hat{\gamma}_k$ and $\hat{\eta}_k$, we can construct

$$\hat{\mathbf{e}}_{-1,k}=\begin{bmatrix}-\cos\hat{\gamma}_k\\ \sin\hat{\gamma}_k\cos\hat{\theta}_{-1,k}e^{j\hat{\eta}_k}\\ -\sin\hat{\gamma}_k\sin\theta_{-1,k}e^{j\hat{\eta}_k}\end{bmatrix}\quad\text{and}\quad\hat{\mathbf{e}}_{0,k}=\begin{bmatrix}-\cos\hat{\gamma}_k\\ \sin\hat{\gamma}_k\cos\hat{\theta}_k^{\mathrm{ref}}e^{j\hat{\eta}_k}\\ -\sin\hat{\gamma}_k\sin\theta_k^{\mathrm{ref}}e^{j\hat{\eta}_k}\end{bmatrix} \tag{37}$$

Thus, $\hat{q}_{-1}(\theta_k,r_k)$ and $\hat{q}_0(\theta_k,r_k)$ can be computed by

$$\hat{q}_{-1}(\theta_k,r_k)=\hat{\mathbf{e}}_{-1,k}^H\hat{\mathbf{a}}_{-1}(\theta_k,\gamma_k,\eta_k,r_k) \tag{38}$$

$$\hat{q}_0(\theta_k,r_k)=\hat{\mathbf{e}}_{0,k}^H\hat{\mathbf{a}}_0(\theta_k,\gamma_k,\eta_k,r_k) \tag{39}$$

Then, as the phase difference between $q_0(\theta_k,r_k)$ and $q_{-1}(\theta_k,r_k)$ satisfies

$$\angle q_{-1}(\theta_k,r_k)-\angle q_0(\theta_k,r_k)=\frac{2\pi}{\lambda}\Delta\sin\theta_k+\frac{\pi}{\lambda r_k}\Delta^2\cos^2\theta_k \tag{40}$$

there would exist a set of estimates of r_k that satisfy (40). These estimates of r_k are computed as

$$\hat{r}_k(n_r)=\frac{\pi\Delta^2\cos^2\hat{\theta}_k}{(\rho_k-\hat{\omega}_k+2\pi n_r)\lambda} \tag{41}$$

$$\hat{\omega}_k=\frac{2\pi}{\lambda}\Delta\sin\hat{\theta}_k \tag{42}$$

$$\left\lceil-\frac{\rho_k-\hat{\omega}_k}{2\pi}\right\rceil\le n_r\le\left\lfloor\frac{\Delta^2}{2\lambda\hat{r}_k^{\mathrm{ref}}}-\frac{\rho_k-\hat{\omega}_k}{2\pi}\right\rfloor \tag{43}$$

$$\rho_k=\angle\hat{q}_{-1}(\theta_k,r_k)-\angle\hat{q}_0(\theta_k,r_k),\quad k=1,\ldots,K \tag{44}$$

where n_r is an integer, and $\hat{\theta}_k$ is the kth signal's disambiguated angle estimate, whose value is derived in the next subsection.

3.5. Disambiguation of cyclically ambiguous angle and range estimates

The reference angle estimates $\{\hat{\theta}_k^{\mathrm{ref}},k=1,\cdots,K\}$ and reference range estimates $\{\hat{r}_k^{\mathrm{ref}},k=1,\ldots,K\}$ are used to resolve the cyclically ambiguous angle estimates $\{\hat{\theta}_k(n_\theta),k=1,\ldots,K\}$ and cyclically ambiguous range estimates $\{\hat{r}_k(n_r),k=1,\cdots,K\}$. The disambiguated angle and range estimates $\hat{\theta}_k$ and $\hat{r}_k$ are found from $\hat{\theta}_k(n_\theta)$ and

(*footnote continued*)
However, for the array geometry considered in this paper, we have $0\le\theta_k<\theta_{-1,k}\le\pi/2$, hence, $\cos\theta_{-1,k}>0$, $\sin^2\theta_{-1,k}-\sin^2\theta_k>0$, and

$$\sin\theta_k\cos\theta_{-1,k}-\sin\theta_{-1,k}\cos\theta_k<\sin\theta_{-1,k}\cos\theta_{-1,k}$$
$$-\sin\theta_{-1,k}\cos\theta_k<\sin\theta_{-1,k}(\cos\theta_{-1,k}-\cos\theta_k)<0$$

Therefore, the solution in (35) is always negative and consequently, it is not a reasonable solution for the range estimate.

$\hat{r}_k(n_r)$, when the value of $|\hat{\theta}_k(n_\theta)-\hat{\theta}_k^{\text{ref}}|$ and $|\hat{r}_k(n_r)-\hat{r}_k^{\text{ref}}|$ are minimized. Mathematically, the disambiguated angle estimates $\hat{\theta}_k$ are

$$\hat{\theta}_k = \arcsin\left(\vartheta_k + n_\theta^o \frac{\lambda}{2\Delta}\right) \tag{45}$$

where n_θ^o is estimated as

$$n_\theta^o = \underset{n_\theta}{\operatorname{argmin}} \left|\hat{\theta}_k^{\text{ref}} - \arcsin\left(\vartheta_k + \frac{n_\theta \lambda}{2\Delta}\right)\right| \tag{46}$$

In an analogous manner, the disambiguated range estimates $\hat{r}_k$ are

$$\hat{r}_k = \frac{\pi\Delta^2 \cos^2\hat{\theta}_k}{(\rho_k - \hat{\omega}_k + 2\pi n_r^o)\lambda} \tag{47}$$

where n_r^o is estimated as

$$n_r^o = \underset{n_r}{\operatorname{argmin}} \left|\hat{r}_k^{\text{ref}} - \frac{\pi\Delta^2 \cos^2\hat{\theta}_k}{(\rho_k - \hat{\omega}_k + 2\pi n_r)\lambda}\right| \tag{48}$$

Note that n_θ^o and n_r^o are determined separately. The search range for n_θ^o and n_r^o are given by (24) and (43), respectively. For n_θ^o and n_r^o, up to a maximum of $\lfloor 4(\Delta/\lambda)+1 \rfloor$ and $\lfloor \Delta^2/(2\lambda\hat{r}_k^{\text{ref}})+2 \rfloor$ candidates are, respectively, tested.[6]

3.6. Implementation of the extended aperture angle-range estimation algorithm

In the discussion above, it is assumed that the cumulant matrices $\mathbf{R}_1$ and $\mathbf{R}_2$ are known exactly. In practical situations, only a finite number of noisy measurements are available for the angle and range estimation. Assuming that the number of signals is known or correctly estimated, the extended aperture angle-range estimation algorithm with the finite tripole array data can be summarized as follows:

(S1) Estimate the cumulant matrices $\hat{\mathbf{R}}_1$ and $\hat{\mathbf{R}}_2$, whose (p,l) th entries are computed by using $\hat{\kappa}_{i,j}^{p,l} = \hat{\xi}_{i,j,p,l} - \hat{\sigma}_{i,j}\hat{\sigma}_{p,l} \;\; -\hat{\sigma}_{i,l}\hat{\sigma}_{p,j} \;\; -\hat{\epsilon}_{i,p}\hat{\epsilon}_{l,j}^*$, where $\hat{\xi}_{i,j,k,\ell} = 1/N\sum_{n=1}^{N} z_i(n) z_j^*(n) \; z_k(n) z_\ell^*(n)$, $\hat{\sigma}_{i,j} = 1/N\sum_{n=1}^{N} z_i(n) \; z_j^*(n)$, and $\hat{\epsilon}_{i,j} = 1/N\sum_{n=1}^{N} z_i(n) \, z_j(n)$. Here, the coefficient $\hat{\kappa}_{i,j}^{p,l}$ is the estimate of the cumulant given in (58).

(S2) Form $\hat{\mathbf{R}} = [\hat{\mathbf{R}}_1^T, \hat{\mathbf{R}}_2^T]^T$; then perform the singular value decomposition on $\hat{\mathbf{R}}$ to construct the $6L \times K$ signal subspace matrix $\hat{\mathbf{E}}_s$, whose columns correspond to the $6L \times 1$ left singular vectors associated with the K largest magnitude singular values of $\hat{\mathbf{R}}$.

(S3) Let $\hat{\mathbf{E}}_1$ and $\hat{\mathbf{E}}_2$ respectively be the first $3L$ and the last $3L$ rows of $\hat{\mathbf{E}}_s$. Perform the eigen-decomposition of $\hat{\mathbf{E}}_1^{\dagger}\hat{\mathbf{E}}_2$.

(S4) Compute the cyclically ambiguous angle estimates $\{\hat{\theta}_k(n_\theta), k = 1, \ldots, K\}$ from (24).

(S5) Estimate $\hat{\mathbf{A}}$ using (25). Calculate $\hat{\theta}_k^{\text{ref}}$, $\hat{\gamma}_k$ and $\hat{\eta}_k$ $(k = 1, \ldots, K)$ using (30), (31) and (32).

(S6) Obtain the disambiguated angle estimates $\{\hat{\theta}_k, k = 1, \ldots, K\}$ using (45) and (46).

(S7) Estimate the reference ranges $\{\hat{r}_k^{\text{ref}}, k = 1, \ldots, K\}$ using (36).

(S8) Estimate the ambiguous ranges $\{\hat{r}_k(n_r), k = 1, \ldots, K\}$ using (41)–(44).

(S9) Obtain the disambiguated range estimates $\{\hat{r}_k, k = 1, \ldots, K\}$ using (47) and (48).

[6] It should be pointed out that the complexity for the disambiguation step is negligible compared to the major complexity for the eigen-decomposition.

Table 1
Maximum number of signals resolvable with an array of $3L$ sensor elements.

Algorithms	Minimum number of sensors
ML algorithm in [8]	$3L-1$
MUSIC-based algorithms in [9,10,12]	$3L-1$
Weighted linear prediction algorithm in [13]	$(3L-1)/2$
Two-step searching algorithm in [14]	$3L$
HOS based algorithms in [16,17]	$3L/2$
HOS based algorithms in [18,19,21]	$3L-1$
The proposed algorithm	$3L-3$

3.7. Remarks

Note that the two sets of angle and range estimates (namely, the coarse reference and cyclically ambiguous estimates) are obtained without performing two-dimensional searching. The cyclically ambiguous angles are estimated from the eigenvalues of $\hat{\mathbf{E}}_1^{\dagger}\hat{\mathbf{E}}_2$, whereas the coarse reference angles, the coarse reference ranges and the cyclically ambiguous ranges are estimated from the eigenvectors of $\hat{\mathbf{E}}_1^{\dagger}\hat{\mathbf{E}}_2$. No mismatch exists between the kth eigenvalue of $\hat{\mathbf{E}}_1^{\dagger}\hat{\mathbf{E}}_2$ and its corresponding eigenvector, which is simply the kth column of the eigenvector matrix $\hat{\mathbf{E}}_1^{\dagger}\hat{\mathbf{E}}_2$. Therefore, the estimated angles and ranges are all automatically matched without any additional matching computation.

Note also that the tripole locations $D_2, \ldots D_{\ell-2}$ can be completely arbitrary and unknown so long as the Fresnel-region environment is preserved. This flexibility compares favorably with most of the other cumulant-based algorithms [15–21], which require the inter-element spacing to be uniform and to be a half wavelength or, a quarter wavelength, or less to avoid the estimation ambiguity.

Moreover, we know from [33] that there may exist $(3L-2)$ steering vectors that are linearly independent for an L-element tripole array. Therefore, the maximum number of signals that can be resolved by the proposed algorithm is $(3L-3)$ with an array of L tripoles. Since each tripole effectively contains a three-element array, the present algorithm in fact requires a total of $3L$ sensor elements to resolve $(3L-3)$ signals. Table 1 gives a detailed comparison with regard to the maximum number of signals resolvable with an array of $3L$ sensor elements. Although the maximum number of signals that can be resolved by the proposed algorithm is slightly less than those which can be resolved by algorithms in [8–10,12,14,18,19,21], the proposed algorithm can estimate the polarization parameters of the signals, while the former algorithms cannot do so.

4. Extension via formulating multiple cumulant matrices with PARAFAC analysis

Note that the cumulant matrices $\mathbf{R}_1$ and $\mathbf{R}_2$ defined in the previous section exploit only the rotational invariance among

the first three tripoles. Even though it is sufficient to define two cumulant matrices to estimate the angles and ranges via ESPRIT, in order to increase the maximum resolvable number of signals and improve the performance of the algorithm, we can also exploit the rotational invariance embedded in the remaining tripoles and utilize parallel factor (PARAFAC) analysis.[7] Since the remaining $(L-3)$ tripoles are arbitrarily located, any two tripoles may be exploited to define a cumulant that produces rotational invariance. For example, the tripoles $\mathbf{z}_i(t)$ and $\mathbf{z}_j(t)$ $(i,j=-1,0,\ldots,L-2)$ can be used to define a cumulant matrix as

$$\mathbf{R}_{i,j}=\sum_{m=1}^{3}\mathrm{cum}(z_{i,m}(t),z_{j,m}^{*}(t),\mathbf{z}(t),\mathbf{z}^{H}(t))=\mathbf{A}\boldsymbol{\Phi}_{i,j}\boldsymbol{\Gamma}\mathbf{A}^{H} \tag{49}$$

where

$$\boldsymbol{\Phi}_{i,j}=\begin{bmatrix}\beta_1^{(i,j)}q_i(\theta_1,r_1)q_j^{*}(\theta_1,r_1) & & \\ & \ddots & \\ & & \beta_K^{(i,j)}q_i(\theta_K,r_K)q_j^{*}(\theta_K,r_K)\end{bmatrix} \tag{50}$$

with

$$\beta_k^{(i,j)}=\frac{\sum_{m=1}^{3}e_m(\theta_{i,k},\gamma_k,\eta_k,r_k)e_m^{*}(\theta_{j,k},\gamma_k,\eta_k,r_k)}{\sum_{m=1}^{3}\left|e_m(\theta_k,\gamma_k,\eta_k,r_k)\right|^2} \tag{51}$$

Note that $\boldsymbol{\Phi}_{i,j}$ depends on the parameter $\beta_k^{(i,j)}$, which is similar to β_k.

Therefore, for an array of L tripoles, $L(L-1)/2$ different pairs of tripoles may be formed to obtain $L(L-1)/2$ different cumulant matrices.[8] Let these matrices be $\mathbf{R}_{0,0}=\mathbf{R}_1$, $\mathbf{R}_{-1,1}=\mathbf{R}_2$, $\mathbf{R}_{-1,0}$, $\mathbf{R}_{-1,2},\ldots,\mathbf{R}_{L-1,L-2}$. Stacking these matrices to get $\mathbf{R}=[\mathbf{R}_{0,0}^T,\mathbf{R}_{-1,1}^T,\ldots,\mathbf{R}_{L-1,L-2}^T]^T$, which can be related to a $3L\times L(L-1)/2\times 3L$ three-way array (TWA) $\underline{\mathbf{R}}$ with a typical element $r_{i,p,j}$ and K-component trilinear decomposition

$$r_{i,p,j}=\sum_{k=1}^{K}a_{i,k}\psi_{p,k}a_{j,k}^{*} \tag{52}$$

$i,j=1,\ldots,3L$, $p=1,\ldots,L(L-1)/2$. In (52), $a_{i,k}$ denotes the (i,k) th element of $3L\times K$ matrix $\mathbf{A}$, and similarly, $\psi_{p,k}$ stands for the (p,k) th element of $L(L-1)/2\times K$ matrix $\boldsymbol{\Psi}$

$$\boldsymbol{\Psi}=\begin{bmatrix}\boldsymbol{\Gamma}_{1,1} & \cdots & \boldsymbol{\Gamma}_{K,K}\\ \boldsymbol{\Gamma}_{1,1}\boldsymbol{\Phi}_{-1,1}^{1,1} & \cdots & \boldsymbol{\Gamma}_{K,K}\boldsymbol{\Phi}_{-1,1}^{K,K}\\ \vdots & \cdots & \vdots\\ \boldsymbol{\Gamma}_{1,1}\boldsymbol{\Phi}_{L-1,L-2}^{1,1} & \cdots & \boldsymbol{\Gamma}_{K,K}\boldsymbol{\Phi}_{L-1,L-2}^{K,K}\end{bmatrix} \tag{53}$$

where $\boldsymbol{\Gamma}_{k,k}$ denotes the (k,k)th entry of the matrix $\boldsymbol{\Gamma}$ and $\boldsymbol{\Phi}_{i,j}^{k,k}$ represents the (k,k)th entry of the matrix $\boldsymbol{\Phi}_{i,j}$. Note that the TWA $\underline{\mathbf{R}}$ can also be expressed via Khatri–Rao matrix product format as

$$\mathbf{R}=(\boldsymbol{\Psi}\odot\mathbf{A})\mathbf{A}^{H} \tag{54}$$

where $\odot$ denotes the Khatri–Rao (column-wise Kronecker) matrix product. Eq. (52) expresses the three-way array $\underline{\mathbf{R}}$ as a sum of K rank-1 terms, defined as the outer product of three vectors; it is known as PARAFAC analysis of $\underline{\mathbf{R}}$. It should be pointed out that Eq. (52) expresses a PARAFAC decomposition of the TWA $\underline{\mathbf{R}}$ if and only if (iff) K is minimal, that is to say iff there is no other trilinear decomposition of $\underline{\mathbf{R}}$ involving less than K rank-1 terms. In other words, the PARAFAC decomposition is a minimal decomposition, which allows us to define the notion of tensor rank. Note that the PARAFAC decomposition of the TWA $\underline{\mathbf{R}}$ would be unique[9] under certain conditions, which are based on the notion of the Kruskal rank (or k-rank) of a matrix[10] [37]. From ([38]), if for $K>1$,[11]

$$2k_{\mathbf{A}}+k_{\boldsymbol{\Psi}}\geq 2K+2 \tag{55}$$

then $\mathbf{A}$ and $\boldsymbol{\Psi}$ are unique up to inherently unresolvable permutation and scaling of columns.[12] The condition (55) can be used to analyze the maximum number of signals that can be resolved from the PARAFAC model (52). Using the fact that the k-rank is always less than or equal to the matrix rank, condition (55) would become

$$2\min\{3L-2,K\}+\min\{L(L-1)/2,K\}\geq 2K+2 \tag{56}$$

Therefore, for $L=3,\ldots,6$, $3L-2>L(L-1)/2$, the trilinear decomposition (52) is unique for any $K\leq 3L-2$; for $K>3L-2$, it is unique for $K\leq 3L-1+L(L-1)/4$. For $L>6$, the trilinear decomposition (52) is unique for any $K\leq 3L-2$; for $3L-2<K\leq L(L-1)/2$, it is unique for $K\leq\min\{6L-6,L(L-1)/2\}$; for $K>L(L-1)/2$, it is unique for $K\leq 3L-1+L(L-1)/4$. These conditions are sufficient for essential uniqueness, but are not always necessary.

The above analysis indicates that the maximum resolvable number of signals can be increased by forming multiple cumulant matrices. For example, for $L=5$, the maximum resolvable number of signals for the ESPRIT-based algorithm in Section 3 is $K=12$, while the maximum resolvable number of signals for the PARAFAC-based algorithm proposed in this section is $K=19$.

To obtain the estimates of the matrices $\mathbf{A}$ and $\boldsymbol{\Psi}$ via trilinear decomposition of (52), several effective algorithms can be used. For a detailed analysis and

[7] The PARAFAC analysis is a multi-way method originating from Hitchcock in 1927 [34]. PARAFAC model, as a useful data analysis tool, is a generalization of the low-rank matrix decomposition to three-way arrays (TWAs) or multi-way arrays (MWAs). During the past decade, the PARAFAC model has gained increasing interest in numerous and diverse applications, such as in scalar sensor array signal processing [35] and communications [36].

[8] The use of only $L(L-1)/2$ matrices $\mathbf{R}_{i,j}$ is to ensure the matrix $\boldsymbol{\Psi}$ to be of full rank. To see this, we have for all $i,j=-1,\ldots,(L-2)$, $\boldsymbol{\Phi}_{i,i}=\boldsymbol{\Phi}_{j,j}$ and $\boldsymbol{\Phi}_{i,j}=\boldsymbol{\Phi}_{j,i}^{*}$. Consequently, if we construct the three-way array using all matrices $\mathbf{R}_{i,j}$, then the full rank of $\boldsymbol{\Psi}$ may not be guaranteed as some of the elements of $\boldsymbol{\Psi}$ are dependent. Since we assume the tripoles to be placed arbitrarily, the elements of $\boldsymbol{\Psi}$ in (53) are independent of one another, thus guaranteeing the matrix $\boldsymbol{\Psi}$ to be of full rank.

[9] This is referred to as essential uniqueness in some works [37,38].

[10] The Kruskal rank (or k-rank) of a matrix $\mathbf{A}$ is $k_{\mathbf{A}}$, if and only if every $k_{\mathbf{A}}$ columns of $\mathbf{A}$ are linearly independent and either $\mathbf{A}$ has $k_{\mathbf{A}}$ columns or $\mathbf{A}$ contains a set of $k_{\mathbf{A}}+1$ linearly dependent columns. Note that the Kruskal rank is always less than or equal to the conventional matrix rank. If $\mathbf{A}$ is of full column rank, then it is also of full k-rank.

[11] For $K=1$, $\mathbf{A}$ and $\boldsymbol{\Psi}$ are always unique.

[12] By extracting the matrix $\mathbf{A}$ using the joint diagonalization methods, uniqueness discussion that is not based on the Kruskal rank is given in [39]. In fact, our uniqueness discussion is based on a conjugate-symmetric PARAFAC model. The resulting uniqueness condition (55) is a combination of the results in [37,36].

comparison of different PARAFAC decomposition methods, one could refer to [40,41]. In this paper, the trilinear alternating least square (TALS) algorithm [35] is adopted. Although the ALS technique has drawbacks such as being non-robust to an overestimated rank or having the presence of correlated factors, it represents a good trade-off between the computational expense and the quality of solution. In TALS, the parameters to be determined are separated into three sets, and each time a least squares cost function that depends only on one set is minimized. With the solution of this linear least squares problem, the subsequent stages of the TALS consist of applying the same principle on the remaining two sets of parameters. The TALS algorithm iterates, changing from one set to the next, until the variation of the loss function or of the parameters is less than a predefined convergence criterion. In the application of the TALS to the problem under consideration, the performance of the TALS algorithm can be improved by exploiting the conjugate-symmetric structure of the PARAFAC model, as used in [51]. In the simulations, the COMFAC algorithm [35] is used to achieve a fast convergence of the TALS algorithm. Note that the classical ALS method provides the PARAFAC decomposition, while the COMFAC algorithm is essentially a fast implementation of the trilinear ALS algorithm. The COMFAC algorithm contains three main parts [36]: (i) compression, (ii) initialization and fitting of PARAFAC in compressed space, and (iii) decompression and refinement in the raw data space. Since all the steps are optimizations in the least squares sense, the TALS/COMFAC algorithm is guaranteed to converge[13] monotonically.

With the estimation of $\mathbf{A}$ and $\mathbf{\Psi}$, the DOAs and ranges of the incoming signals can be easily estimated from the steps given in Section 3. It is noted that the method used here for identification of the matrix $\mathbf{A}$, which is based on the PARAFAC decomposition of a fourth-order-cumulant-based multi-way array, has also been widely used in solving many other independent component analysis (ICA) and blind identification of mixtures (BIM) problems [42–51]. In fact, the PARAFAC decomposition of a three-way array that has two loading matrices, which are conjugates of each other, is equivalent to the joint diagonalization by congruence of matrix slices extracted from the three-way array. Cardoso and Souloumiac [44] were the first ones to propose a method based on an orthogonal joint diagonalization scheme [52] for joint diagonalization of fourth-order-cumulant-based matrices. In contrast, Yeredor [51] proposed the joint diagonalization of such matrices with a non-orthogonal joint diagonalization method, which allows us to identify underdetermined mixtures.

It is also noted that the method for the estimation of the matrix $\mathbf{A}$ from two $3L\times 3L$ matrices in Section 3 consists of the PARAFAC decomposition of a three-way array of size $3L\times 2\times 3L$. Thus, the TALS/COMFAC algorithm can also be applied to estimate $\mathbf{A}$ from this $3L\times 2\times 3L$ three-way array. In addition, unlike the TALS/COMFAC algorithm, the method presented in Section 3 is in fact the classical generalized rank annihilation method (GRAM) [53], which is a non-iterative method.

[13] This is a local convergence.

5. Simulations

Monte Carlo simulations are presented to illustrate the performance of the proposed cumulant-based extended aperture angle-range estimation algorithm relative to the cumulant-based angle-range estimation with a scalar-sensor array [18], the cumulant-based angle-range estimation with a cross-dipole array [19] and the performance of the CRB for the proposed algorithm (derived in Appendix B). For the proposed algorithm, an irregularly spaced linear array of six identical isotropic tripoles are placed at $-2, 0, 2, 2.5, 3, 3.25$ wavelengths from the origin of the array axis. For the algorithm in [18], an 18-element uniformly-spaced scalar-sensor array with a spacing of $\lambda/4$ is used, and for the algorithm in [19], a 9-element uniformly spaced cross-dipole array with a spacing of $\lambda/4$ is used; hence, the total number of sensor elements is the same for all the three algorithms. For the algorithms in [18] and [19], the estimated sets of angles and ranges are assumed to have been correctly paired. In all the figures, we use the labels "ESPRIT" for the algorithm presented in Section 3, "PARAFAC-1" for the algorithm that estimates the matrix $\mathbf{A}$ from the $3L\times 2\times 3L$ three-way array $[\mathbf{R}_1^T,\mathbf{R}_2^T]^T$ by PARAFAC decomposition, and "PARAFAC-2" for the extended algorithm presented in Section 4. We assume that incident upon the aforementioned sensor-array are two uncorrelated narrowband non-Gaussian monochromatic signals from the Fresnel-region, with their arriving angles and ranges: $\theta_1=10^\circ$, $\theta_2=20^\circ$, $r_1=8\lambda$, and $r_2=10\lambda$. The first signal is left-circularly polarized and the second right-circularly polarized, i.e., $\gamma_1=45^\circ$, $\eta_1=90^\circ$, $\gamma_2=45^\circ$, $\eta_2=-90^\circ$. The additive noise is assumed to be spatial white complex Gaussian, and the signal-to-noise ratio (SNR) is defined relative to each signal. In each of the following simulations, we generate five hundreds independent Monte Carlo trials. The performance metrics used are the root mean squared errors (RMSEs) of the two signals, which are defined as

$$\mathrm{RMSE}_{\theta_i}=\sqrt{\frac{1}{M}\sum_{m=1}^{M}(\hat{\theta}_i(m)-\theta_i)^2},\quad \mathrm{RMSE}_{r_i}=\sqrt{\frac{1}{M}\sum_{m=1}^{M}(\hat{r}_i(m)-r_i)^2} \tag{57}$$

for the angle and the range, respectively, where $\hat{\theta}_i(m)$ and $\hat{r}_i(m)$ are the angle and the range of the ith signal estimated from the mth Monte Carlo trial, and M is the number of total Monte Carlo trials.

Figs. 2 and 3 show the RMSEs of the proposed cumulant-based extended aperture angle-range estimation algorithm and the algorithms in [18,19] as functions of the SNR varying from 0 dB to 40 dB in steps of 5 dB. The number of snapshots is fixed at $N=1000$. From these two figures, we see that when the SNR is greater than 7 dB, the proposed algorithm has an estimation accuracy that is significantly higher than those of the other two algorithms. For the proposed algorithm (ESPRIT), the polarization parameters of the signals are also estimated as shown in Table 2 by using the analytical equations given in (31)

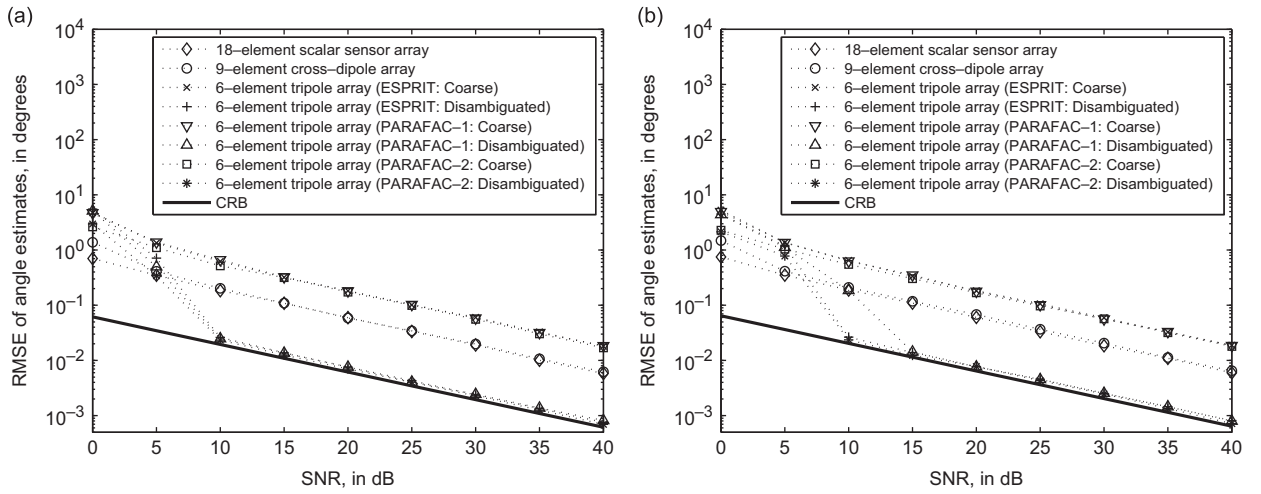

Fig. 2. (a) RMSEs of θ_1 estimates against SNR. (b) RMSEs of θ_2 estimates against SNR. Two monochromatic signals with digital frequencies $f_1=0.1, f_2=0.4$ and arriving parameters $\theta_1=10^\circ$, $\theta_2=20^\circ$, $r_1=8\lambda$, $r_2=10\lambda$ impinge upon the array, and $M=500$ per data point.

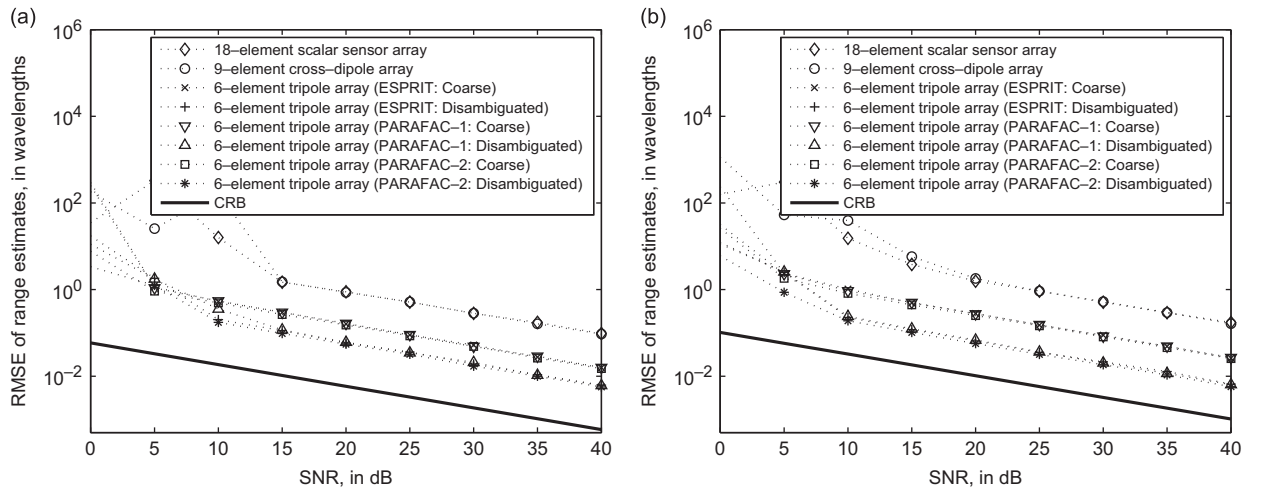

Fig. 3. (a) RMSEs of r_1 estimates against SNR. (b) RMSEs of r_2 estimates against SNR. Two monochromatic signals with digital frequencies $f_1=0.1, f_2=0.4$ and arriving parameters $\theta_1=10^\circ$, $\theta_2=20^\circ$, $r_1=8\lambda$, $r_2=10\lambda$ impinge upon the array, and $M=500$ per data point.

Table 2
Estimated polarization parameters.

Parameters	SNR						
	0 dB	5 dB	10 dB	15 dB	20 dB	25 dB	30 dB
$\hat{\gamma}_1$	42.93°	44.81°	44.95°	44.99°	44.99°	45.00°	45.00°
$\hat{\gamma}_2$	40.91°	44.71°	44.92°	44.99°	44.99°	45.00°	45.00°
$\hat{\eta}_1$	88.86°	89.91°	89.91°	89.89°	90.02°	90.07°	90.00°
$-\hat{\eta}_2$	90.14°	89.99°	90.03°	89.98°	89.96°	90.01°	90.00°

and (32). It is observed from Table 2 that the proposed algorithm can successfully estimate the polarization parameters of the signals when the SNR is 5 dB or above. Note that the algorithms in [18,19] cannot estimate the polarization parameters of the signals.

Figs. 4 and 5 show the RMSEs of the proposed algorithm and those in [18,19] as functions of the number of snapshots, varying from 20 to 2000. The SNR is set at 15 dB. From these figures, it is seen that RMSEs of the angle and the range estimates decrease as the number of snapshots increases. In addition, when the snapshot number is not very small, the proposed cumulant-based extended aperture angle-range estimation algorithm has a performance that is superior to the other two algorithms in terms of lower RMSEs.

Fig. 6 shows, for the proposed algorithm and those in [18,19], the RMSEs of the angle estimates of the first signal as functions of the arrival angles θ_2 of the second signal, varying from 10.5° to 37°. The remaining signal parameters are set as $\theta_1=10^\circ$, $r_1=r_2=8\lambda$, $\gamma_1=\gamma_2=45^\circ$, $\eta_1=-\eta_2=90^\circ$. The SNR and the number of snapshots are fixed at 15 dB and 1000, respectively. It is seen from Fig. 6 that the estimation errors of the proposed algorithm remain almost unchanged as the arrival angle θ_2 varies. In contrast, the algorithms in [18,19] perform poorly when the two signals are very closely spaced.

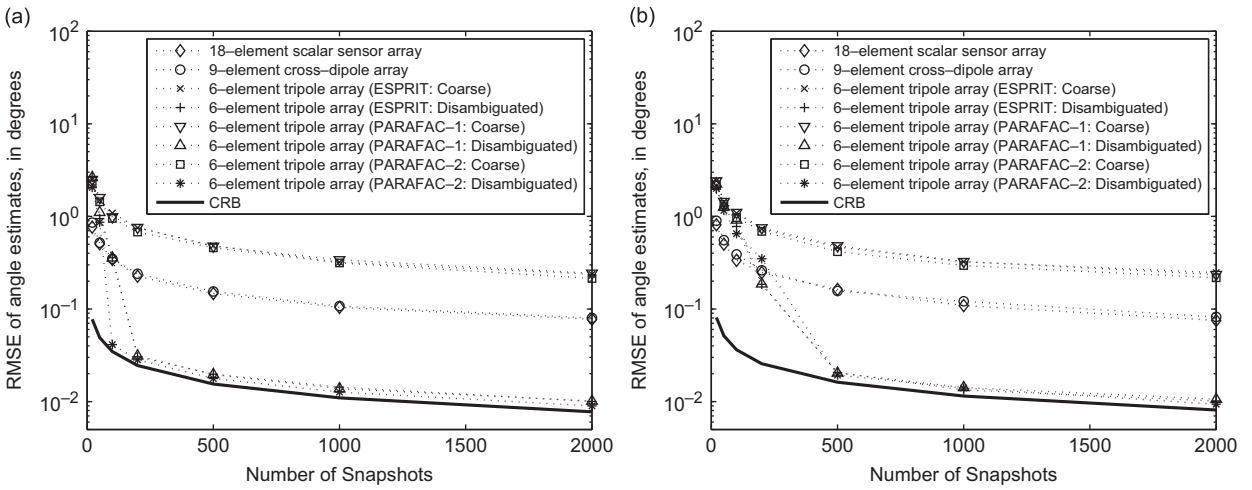

Fig. 4. (a) RMSEs of θ_1 estimates against snapshots. (b) RMSEs of θ_2 estimates against snapshots. Two monochromatic signals with digital frequencies $f_1=0.1, f_2=0.4$ and arriving parameters $\theta_1=10^\circ$, $\theta_2=20^\circ$, $r_1=8\lambda$, $r_2=10\lambda$ impinge upon the array, SNR=15 dB, and $M=500$ per data point.

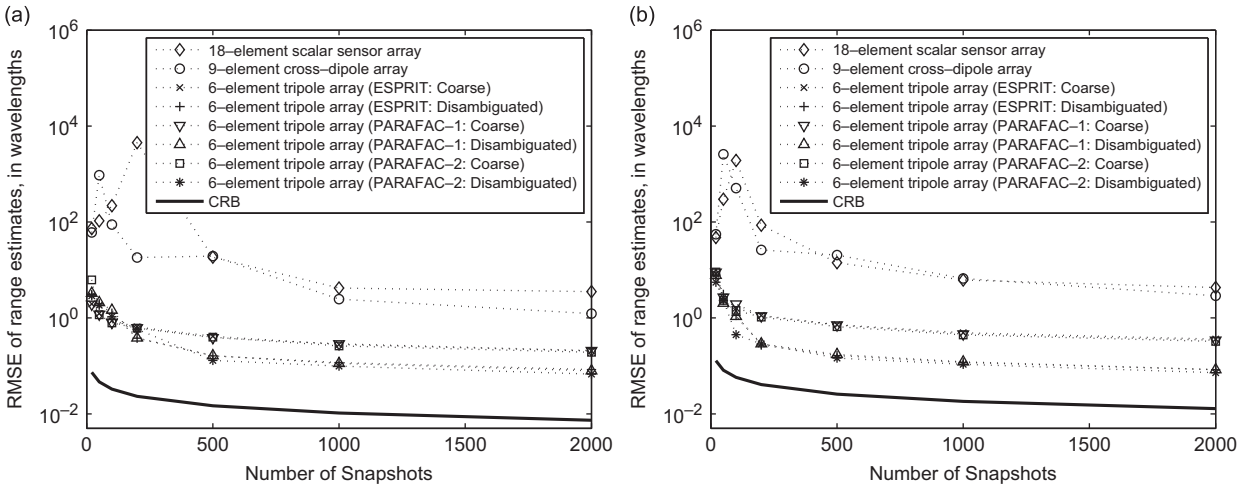

Fig. 5. (a) RMSEs of r_1 estimates against snapshots. (b) RMSEs of r_2 estimates against snapshots. Two monochromatic signals with digital frequencies $f_1=0.1, f_2=0.4$ and arriving parameters $\theta_1=10^\circ$, $\theta_2=20^\circ$, $r_1=8\lambda$, $r_2=10\lambda$ impinge upon the array, SNR=15 dB, and $M=500$ per data point.

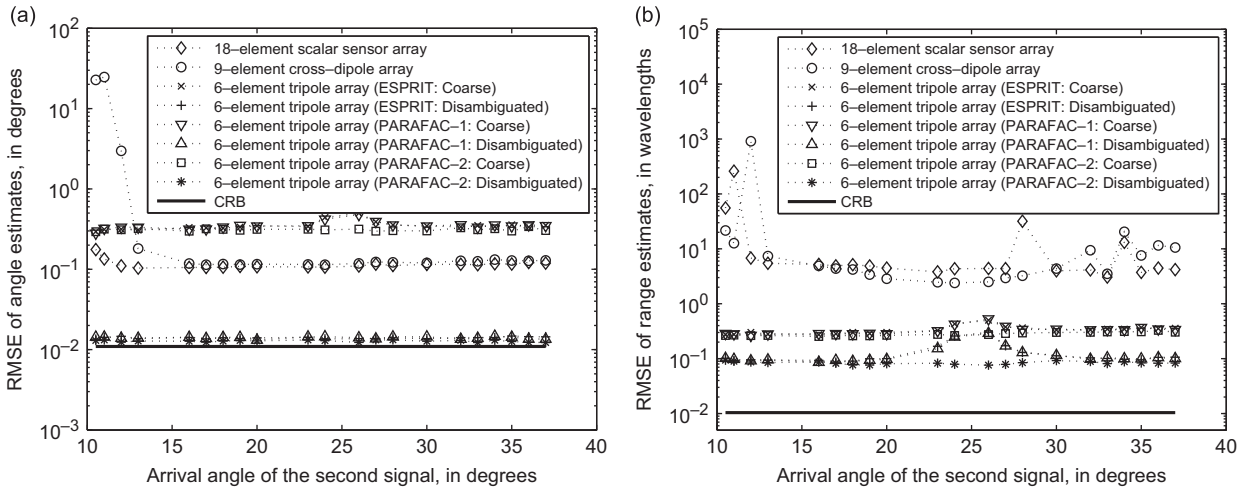

Fig. 6. (a) RMSEs of θ_1 estimates against the arrival angle θ_2. (b) RMSEs of r_1 estimates against the arrival angle θ_2. Two monochromatic signals with digital frequencies $f_1=0.1, f_2=0.4$ and arriving parameters $\theta_1=10^\circ$, $r_1=r_2=8\lambda$ impinge upon the array, and $M=500$ per data point.

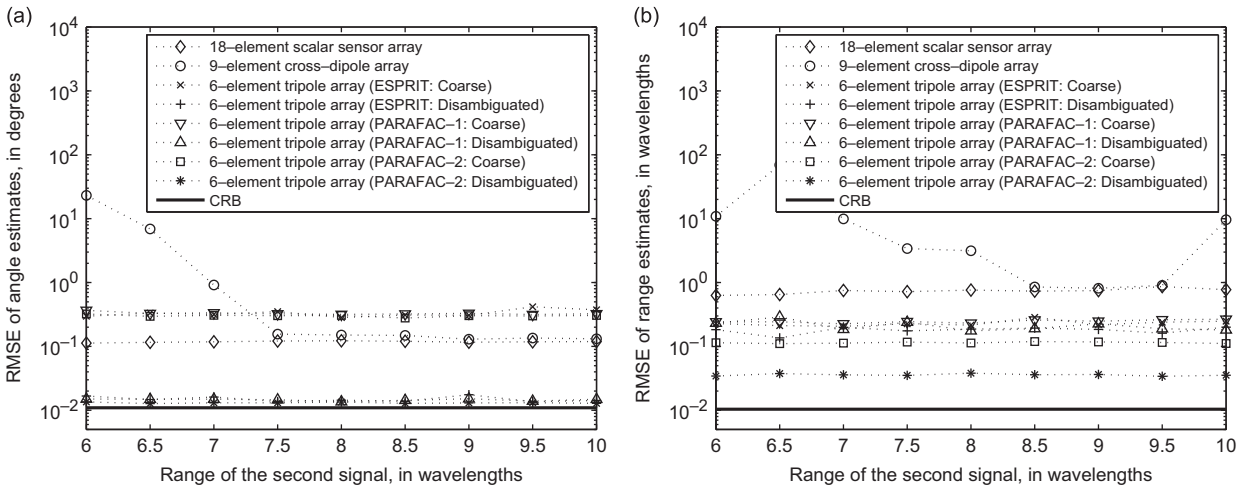

Fig. 7. (a) RMSEs of θ_1 estimates against the arrival range r_2. (b) RMSEs of r_1 estimates against the arrival range r_2. Two monochromatic signals with digital frequencies $f_1=0.1, f_2=0.4$ and arriving parameters $\theta_1=\theta_2=10^\circ$, $r_1=5\lambda$ impinge upon the array, and $M=500$ per data point.

Fig. 7 shows, for the proposed algorithm and those in [18,19], the RMSEs of the estimates of the first signal as functions of the arrival ranges r_2 of the second signal, varying from 6λ to 10λ. The remaining signal parameters are set as $\theta_1=\theta_2=10^\circ$, $r_1=5\lambda$, $\gamma_1=\gamma_2=45^\circ$, $\eta_1=-\eta_2=90^\circ$. The SNR and the number of snapshots are fixed at 15 dB and 1000, respectively. We can see that the proposed algorithm outperforms the algorithms in [18,19] and is insensitive to changes in the range parameter of the second signal.

From Figs. 2 to 7, it is seen that the "PARAFAC-1" and the "ESPRIT" provide almost the same performance. Moreover, the "PARAFAC-2" performs better than the "ESPRIT" and "PARAFAC-1", especially for the scenario in Fig. 7. The RMSEs of the angles of all the three algorithms are very close to the CRB, while those of the ranges are not. This can be explained as follows: the estimation of the ranges is based on the previous estimations of the angles of arrival, and the errors in the estimation of the angles are "propagated" in the estimation of the ranges.

Fig. 8 shows that for an array of $L=3$ tripoles, the proposed algorithm can resolve up to $3(L-1)=6$ signals. The tripoles are placed at $-2,0,2$ wavelengths from the origin of the array axis. The six signals arrive with the following parameters: $\{\theta_1,\theta_2,\theta_3,\ \theta_4,\theta_5,\theta_6\}=\{5^\circ,15^\circ,25^\circ,25^\circ,\ 35^\circ,45^\circ\}$, $\{r_1,r_2,r_3,\ r_4,r_5,r_6\}=\{4\lambda,6\lambda,\ 8\lambda,4\lambda,\ 6\lambda,4\lambda\}$ and $\gamma_1=\gamma_2=\ \gamma_3=\gamma_4=\gamma_5=\gamma_6=45^\circ$, $\eta_1=\eta_5=-\eta_2=-\eta_6=90^\circ$, $\eta_3=\eta_4=0^\circ$. The SNR and the number of snapshots are fixed at 30 dB and 1000, respectively. It is noteworthy that the proposed algorithm can resolve signals with identical angles of arrival ($\theta_3=\theta_4=25^\circ$), or identical ranges ($r_1=r_4=r_6=4\lambda$).

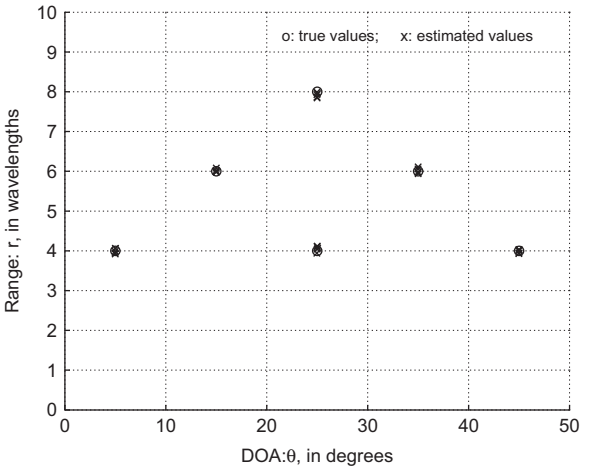

Fig. 8. Angle and range estimates for five independent runs. Six monochromatic signals with digital frequencies $\{f_1,f_2,f_3,\ f_4,f_5,f_6\}=\{0.1,0.12,0.23,0.31,0.41,0.47\}$ and arriving parameters $\{\theta_1,\theta_2,\theta_3,\ \theta_4,\theta_5,\theta_6\}=\{5^\circ,15^\circ,25^\circ,25^\circ,\ 35^\circ,45^\circ\}$ and $\{r_1,r_2,r_3,\ r_4,r_5,r_6\}=\{4\lambda,6\lambda,\ 8\lambda,4\lambda,\ 6\lambda,4\lambda\}$, impinge upon the three tripole array.

6. Conclusion

A method to extend the aperture for estimating the angles and ranges of multiple Fresnel-region sources has been proposed using a linear tripole array. Two cumulant-based matrices have been defined to estimate the DOA and the range of each of the sources from its tripole steering vector by using the ESPRIT technique. These DOA and range estimates are then used as coarse reference estimates to disambiguate the cyclic phase ambiguities induced from the spatial phase factors when the inter-sensor spacing exceeds a half wavelength. Unlike most of the other cumulant-based algorithms, the proposed extended aperture angle-range estimation algorithm requires neither two-dimensional searching nor parameter pairing, and can resolve up to $3(L-1)$ sources with L tripoles. It should be pointed out that to the best of our knowledge, all the previous solutions for the Fresnel-region angle and range estimation problem assume the inter-sensor spacings are within a quarter or a half wavelength to guarantee unique and unambiguous angle and range estimates. The present algorithm has considered, for the first time, the sensor spacing to be more than a half wavelength in the Fresnel-region angle and range

estimation problem. Hence, an extension of the array aperture has been achieved for the Fresnel-region parameter estimation problem. In addition, since the fourth-order cumulant can suppress correlated noise, the proposed algorithm is robust in the presence of uncorrelated or spatially correlated noise, as long as the noise has zero fourth order cumulants.

Appendix A. Derivations of (13) and (14)

Define $b_{\ell,m,k}=e_m(\theta_{\ell,k},\gamma_k,\eta_k,r_k)q_\ell(\theta_k,r_k)$, then from the assumptions II–IV and the cumulant properties CP1, CP3, CP4, CP5 in [31], we have

$$\begin{aligned}&\mathrm{cum}(z_{i,m}(t),z^*_{j,m}(t),z_{p,m}(t),z^*_{l,m}(t))\\&=\sum_{k=1}^{K}\mathrm{cum}(b_{i,m,k}s_k(t),b^*_{j,m,k}s^*_k(t),b_{p,m,k}s_k(t),b^*_{l,m,k}s^*_k(t))\\&=\sum_{k=1}^{K}b_{i,m,k}b^*_{j,m,k}b_{p,m,k}b^*_{l,m,k}\mathrm{cum}(s_k(t),s^*_k(t),s_k(t),s^*_k(t))\\&=\sum_{k=1}^{K}b_{i,m,k}b^*_{j,m,k}b_{p,m,k}b^*_{l,m,k}\zeta_k\end{aligned}\tag{58}$$

Written in matrix form, the right side of the above equation becomes

$$[b_{p,m,1},\ldots,b_{p,m,K}]\begin{bmatrix}b_{i,m,1}b^*_{j,m,1}\zeta_1&&\\&\ddots&\\&&b_{i,m,K}b^*_{j,m,K}\zeta_K\end{bmatrix}[b_{l,m,1},\ldots,b_{l,m,K}]^H\tag{59}$$

Since the matrix $\mathbf{A}$ can be expressed as

$$\mathbf{A}=\begin{bmatrix}b_{-1,1,1}&b_{-1,1,2}&\cdots&b_{-1,1,K}\\b_{-1,2,1}&b_{-1,2,2}&\cdots&b_{-1,2,K}\\b_{-1,3,1}&b_{-1,3,2}&\cdots&b_{-1,3,K}\\b_{0,1,1}&b_{0,1,2}&\cdots&b_{0,1,K}\\\vdots&\vdots&\cdots&\vdots\\b_{L-2,1,1}&b_{L-2,1,2}&\cdots&b_{L-2,1,K}\\b_{L-2,2,1}&b_{L-2,2,2}&\cdots&b_{L-2,2,K}\\b_{L-2,3,1}&b_{L-2,3,2}&\cdots&b_{L-2,3,K}\end{bmatrix}\tag{60}$$

we can get

$$\mathrm{cum}(z_{0,m}(t),z^*_{0,m}(t),\mathbf{z}(t),\mathbf{z}^H(t))=\mathbf{A}\begin{bmatrix}|b_{0,m,1}|^2\zeta_1&&\\&\ddots&\\&&|b_{0,m,K}|^2\zeta_K\end{bmatrix}\mathbf{A}^H\tag{61}$$

which yields

$$\mathbf{R}_1=\mathbf{A}\begin{bmatrix}\sum_{m=1}^{3}|b_{0,m,1}|^2\zeta_1&&\\&\ddots&\\&&\sum_{m=1}^{3}|b_{0,m,K}|^2\zeta_K\end{bmatrix}\mathbf{A}^H=\mathbf{A}\mathbf{\Gamma}\mathbf{A}^H\tag{62}$$

and

$$\begin{aligned}&\mathrm{cum}(z_{-1,m}(t),z^*_{1,m}(t),\mathbf{z}(t),\mathbf{z}^H(t))=\\&\mathbf{A}\begin{bmatrix}b_{-1,m,1}b^*_{1,m,1}\zeta_1&&\\&\ddots&\\&&b_{-1,m,K}b^*_{1,m,K}\zeta_K\end{bmatrix}\mathbf{A}^H\\&=\mathbf{A}\begin{bmatrix}\frac{b_{-1,m,1}b^*_{1,m,1}}{|b_{0,m,1}|^2}|b_{0,m,1}|^2\zeta_1&&\\&\ddots&\\&&\frac{b_{-1,m,K}b^*_{1,m,K}}{|b_{0,m,K}|^2}|b_{0,m,K}|^2\zeta_K\end{bmatrix}\mathbf{A}^H\end{aligned}\tag{63}$$

which yields

$$\mathbf{R}_2=\mathbf{A}\mathbf{\Lambda}\mathbf{\Gamma}\mathbf{A}^H\tag{64}$$

where

$$\mathit{\Lambda}=\begin{bmatrix}\frac{\sum_{m=1}^{3}b_{-1,m,1}b^*_{1,m,1}}{\sum_{m=1}^{3}|b_{0,m,1}|^2}&&\\&\ddots&\\&&\frac{\sum_{m=1}^{3}b_{-1,m,K}b^*_{1,m,K}}{\sum_{m=1}^{3}|b_{0,m,K}|^2}\end{bmatrix}\tag{65}$$

The entries in $\mathit{\Lambda}$ are of the form

$$\begin{aligned}&\frac{\sum_{m=1}^{3}b_{-1,m,k}b^*_{1,m,k}}{\sum_{m=1}^{3}|b_{0,m,k}|^2}\\&=\frac{\sum_{m=1}^{3}e_m(\theta_{-1,k},\gamma_k,\eta_k,r_k)e^*_m(\theta_{1,k},\gamma_k,\eta_k,r_k)}{\sum_{m=1}^{3}|e_m(\theta_k,\gamma_k,\eta_k,r_k)|^2}e^{j(4\pi/\lambda)\mathit{\Delta}\sin\theta_k}\end{aligned}\tag{66}$$

Note that

$$\frac{\sum_{m=1}^{3}e_m(\theta_{-1,k},\gamma_k,\eta_k,r_k)e^*_m(\theta_{1,k},\gamma_k,\eta_k,r_k)}{\sum_{m=1}^{3}|e_m(\theta_k,\gamma_k,\eta_k,r_k)|^2}$$

is real-valued. Letting

$$\beta_k=\frac{\sum_{m=1}^{3}e_m(\theta_{-1,k},\gamma_k,\eta_k,r_k)e^*_m(\theta_{1,k},\gamma_k,\eta_k,r_k)}{\sum_{m=1}^{3}|e_m(\theta_k,\gamma_k,\eta_k,r_k)|^2}\tag{67}$$

we see that $\mathbf{\Lambda}=\mathbf{\Phi}$ (as defined in (16)). Hence, the relation (14), namely, $\mathbf{R}_2=\mathbf{A}\mathbf{\Phi}\mathbf{\Gamma}\mathbf{A}^H$ is established.

Appendix B. Derivation of the Cramér–Rao bound

The Cramér–Rao Bound (CRB) analysis in [12,13] assumes the set of all incident signals to be statistically independent, zero-mean complex-Gaussian random sequences. These signal models are not applicable to the present scenario, where the set of incident signals are non-Gaussian. Moreover, [12,13] employ the scalar sensor array, whereas the present paper considers the tripole array. This section derives the CRB for the Fresnel-region angle-range estimation with a tripole array. The following simple assumptions have been made about the statistical model of the data in Section 2: K monochromatic signals impinge upon an array of L linear tripoles; the data samples are obtained at time instants $t=nT_s$, where T_s refers to the time-sampling period; the noise of each tripole and each element of a tripole is additive zero-mean spatio-temporally uncorrelated with a

Gaussian distribution. Note that this statistical model is the same as the one considered in the simulations. Further, the frequencies and initial phases of the signals are presumed as known constants. The $3L \times 3L$ noise covariance-matrix $\mathbf{\Gamma}_0$ is unknown, deterministic, diagonal with all diagonal elements equal to σ^2, which represents the noise-variance at each of the antenna components.

With N data samples, the total data-set can be formed as a $3LN \times 1$ vector $\boldsymbol{\zeta}$

$$\boldsymbol{\zeta} = \boldsymbol{\mu} + \boldsymbol{v} \tag{68}$$

in which

$$\boldsymbol{\mu} = \sum_{k=1}^{K} \mathbf{s}_k \otimes \mathbf{a}_k \tag{69}$$

$$\boldsymbol{v} = [\mathbf{n}^T(T_s), \mathbf{n}^T(2T_s), \ldots \mathbf{n}^T(NT_s)]^T \tag{70}$$

where $\mathbf{a}_k = \mathbf{a}(\theta_k, \gamma_k, \eta_k, r_k)$, $\mathbf{s}_k = e^{j\epsilon_k}[e^{j2\pi f_k T_s}, e^{j4\pi f_k T_s}, \ldots, e^{j2N\pi f_k T_s}]^T$, where ϵ_k and f_k are, respectively, the initial phase and digital frequency of the kth signal, and $\boldsymbol{v}$ denotes the $3LN \times 1$ noise vector with covariance matrix $\mathbf{\Gamma}_n = \mathbf{I}_N \otimes \mathbf{\Gamma}_0$, where $\mathbf{I}_N$ is a $N \times N$ identity matrix. Therefore, $\boldsymbol{\zeta}$ is a Gaussian vector with mean $\boldsymbol{\mu}$ and covariance $\mathbf{\Gamma}_n$.

Define a $4K \times 1$ unknown parameter vector $\boldsymbol{\theta} = [\boldsymbol{\theta}_1^T, \ldots, \boldsymbol{\theta}_K^T]^T$, where $\boldsymbol{\theta}_k = [\theta_k, \gamma_k, \eta_k, r_k]^T$. Then, the $4K \times 4K$ *Fisher information matrix* (FIM) is given by [54]

$$\mathbf{J}(\boldsymbol{\theta}) = 2\Re\left[\left(\frac{\partial \boldsymbol{\mu}}{\partial \boldsymbol{\theta}}\right)^H \mathbf{\Gamma}_n^{-1}\left(\frac{\partial \boldsymbol{\mu}}{\partial \boldsymbol{\theta}}\right)\right] \tag{71}$$

where the elements of $\partial\boldsymbol{\mu}/\partial\boldsymbol{\theta}$ are

$$\frac{\partial \boldsymbol{\mu}}{\partial \theta_k} = \mathbf{s}_k \otimes \frac{\partial \mathbf{a}_k}{\partial \theta_k} = \mathbf{s}_k \otimes \begin{bmatrix} \frac{\partial q_{-1,k}}{\partial \theta_k}\mathbf{e}_{-1,k} + q_{-1,k}\frac{\partial \mathbf{e}_{-1,k}}{\partial \theta_k} \\ \frac{\partial \mathbf{e}_{0,k}}{\partial \theta_k} \\ \vdots \\ \frac{\partial q_{L-2,k}}{\partial \theta_k}\mathbf{e}_{L-2,k} + q_{L-2,k}\frac{\partial \mathbf{e}_{L-2,k}}{\partial \theta_k} \end{bmatrix} \tag{72}$$

$$\frac{\partial \boldsymbol{\mu}}{\partial \gamma_k} = \mathbf{s}_k \otimes \frac{\partial \mathbf{a}_k}{\partial \gamma_k} = \mathbf{s}_k \otimes \begin{bmatrix} q_{-1,k}\frac{\partial \mathbf{e}_{-1,k}}{\partial \gamma_k} \\ \frac{\partial \mathbf{e}_{0,k}}{\partial \gamma_k} \\ \vdots \\ q_{L-2,k}\frac{\partial \mathbf{e}_{L-2,k}}{\partial \gamma_k} \end{bmatrix} \tag{73}$$

$$\frac{\partial \boldsymbol{\mu}}{\partial \eta_k} = \mathbf{s}_k \otimes \frac{\partial \mathbf{a}_k}{\partial \eta_k} = \mathbf{s}_k \otimes \begin{bmatrix} q_{-1,k}\frac{\partial \mathbf{e}_{-1,k}}{\partial \eta_k} \\ \frac{\partial \mathbf{e}_{0,k}}{\partial \eta_k} \\ \vdots \\ q_{L-2,k}\frac{\partial \mathbf{e}_{L-2,k}}{\partial \eta_k} \end{bmatrix} \tag{74}$$

$$\frac{\partial \boldsymbol{\mu}}{\partial r_k} = \mathbf{s}_k \otimes \frac{\partial \mathbf{a}_k}{\partial r_k} = \mathbf{s}_k \otimes \begin{bmatrix} \frac{\partial q_{-1,k}}{\partial r_k}\mathbf{e}_{-1,k} + q_{-1,k}\frac{\partial \mathbf{e}_{-1,k}}{\partial r_k} \\ \frac{\partial \mathbf{e}_{0,k}}{\partial r_k} \\ \vdots \\ \frac{\partial q_{L-2,k}}{\partial r_k}\mathbf{e}_{L-2,k} + q_{L-2,k}\frac{\partial \mathbf{e}_{L-2,k}}{\partial r_k} \end{bmatrix} \tag{75}$$

where $q_{\ell,k} = q_\ell(\theta_k, r_k), \ell = -1, 0, \ldots, L-2$. We now express $\mathbf{J}(\boldsymbol{\theta})$ in a block matrix form

$$\mathbf{J}(\boldsymbol{\theta}) = \begin{bmatrix} \mathbf{J}_{1,1} & \cdots & \mathbf{J}_{1,K} \\ \vdots & \vdots & \vdots \\ \mathbf{J}_{K,1} & \cdots & \mathbf{J}_{K,K} \end{bmatrix} \tag{76}$$

where the (i,j) th block equals

$$\mathbf{J}_{i,j} = \begin{bmatrix} J_{\theta_i,\theta_j} & J_{\theta_i,\gamma_j} & J_{\theta_i,\eta_j} & J_{\theta_i,r_j} \\ J_{\gamma_i,\theta_j} & J_{\gamma_i,\gamma_j} & J_{\gamma_i,\eta_j} & J_{\gamma_i,r_j} \\ J_{\eta_i,\theta_j} & J_{\eta_i,\gamma_j} & J_{\eta_i,\eta_j} & J_{\eta_i,r_j} \\ J_{r_i,\theta_j} & J_{r_i,\gamma_j} & J_{r_i,\eta_j} & J_{r_i,r_j} \end{bmatrix} \tag{77}$$

Let $e_{\ell,m,i} = e_m(\theta_{\ell,i}, \gamma_i, \eta_i, r_i)$. Then for $i=j$, we have

$$\mathbf{J}_{i,i} = \begin{bmatrix} \frac{2N}{\sigma^2}M_{\theta_i,\theta_i} & \frac{2N}{\sigma^2}M_{\theta_i,\gamma_i} & \frac{2N}{\sigma^2}M_{\theta_i,\eta_i} & \frac{2N}{\sigma^2}M_{\theta_i,r_i} \\ \frac{2N}{\sigma^2}M_{\gamma_i,\theta_i} & \frac{2N}{\sigma^2}M_{\gamma_i,\gamma_i} & \frac{2N}{\sigma^2}M_{\gamma_i,\eta_i} & \frac{2N}{\sigma^2}M_{\gamma_i,r_i} \\ \frac{2N}{\sigma^2}M_{\eta_i,\theta_i} & \frac{2N}{\sigma^2}M_{\eta_i,\gamma_i} & \frac{2N}{\sigma^2}M_{\eta_i,\eta_i} & \frac{2N}{\sigma^2}M_{\eta_i,r_i} \\ \frac{2N}{\sigma^2}M_{r_i,\theta_i} & \frac{2N}{\sigma^2}M_{r_i,\gamma_i} & \frac{2N}{\sigma^2}M_{r_i,\eta_i} & \frac{2N}{\sigma^2}M_{r_i,r_i} \end{bmatrix} \tag{78}$$

where

$$M_{\theta_i,\theta_i} = \sum_{\ell=-1}^{L-2}\sum_{m=1}^{3}\left|\frac{\partial q_{\ell,i}}{\partial \theta_i}e_{\ell,m,i} + q_{\ell,i}\frac{\partial e_{\ell,m,i}}{\partial \theta_i}\right|^2 \tag{79}$$

$$M_{\theta_i,\gamma_i} = \sum_{\ell=-1}^{L-2}\sum_{m=1}^{3}\left(\frac{\partial q_{\ell,i}}{\partial \theta_i}e_{\ell,m,i} + q_{\ell,i}\frac{\partial e_{\ell,m,i}}{\partial \theta_i}\right)^*\left(q_{\ell,i}\frac{\partial e_{\ell,m,i}}{\partial \gamma_i}\right) \tag{80}$$

$\vdots$

and for $i \neq j$

$$\mathbf{J}_{i,j} = \begin{bmatrix} \frac{2}{\sigma^2}\mathbf{s}_i^H\mathbf{s}_j M_{\theta_i,\theta_j} & \frac{2}{\sigma^2}\mathbf{s}_i^H\mathbf{s}_j M_{\theta_i,\gamma_j} & \frac{2}{\sigma^2}\mathbf{s}_i^H\mathbf{s}_j M_{\theta_i,\eta_j} & \frac{2}{\sigma^2}\mathbf{s}_i^H\mathbf{s}_j M_{\theta_i,r_j} \\ \frac{2}{\sigma^2}\mathbf{s}_i^H\mathbf{s}_j M_{\gamma_i,\theta_j} & \frac{2}{\sigma^2}\mathbf{s}_i^H\mathbf{s}_j M_{\gamma_i,\gamma_j} & \frac{2}{\sigma^2}\mathbf{s}_i^H\mathbf{s}_j M_{\gamma_i,\eta_j} & \frac{2}{\sigma^2}\mathbf{s}_i^H\mathbf{s}_j M_{\gamma_i,r_j} \\ \frac{2}{\sigma^2}\mathbf{s}_i^H\mathbf{s}_j M_{\eta_i,\theta_j} & \frac{2}{\sigma^2}\mathbf{s}_i^H\mathbf{s}_j M_{\eta_i,\gamma_j} & \frac{2}{\sigma^2}\mathbf{s}_i^H\mathbf{s}_j M_{\eta_i,\eta_j} & \frac{2}{\sigma^2}\mathbf{s}_i^H\mathbf{s}_j M_{\eta_i,r_j} \\ \frac{2}{\sigma^2}\mathbf{s}_i^H\mathbf{s}_j M_{r_i,\theta_j} & \frac{2}{\sigma^2}\mathbf{s}_i^H\mathbf{s}_j M_{r_i,\gamma_j} & \frac{2}{\sigma^2}\mathbf{s}_i^H\mathbf{s}_j M_{r_i,\eta_j} & \frac{2}{\sigma^2}\mathbf{s}_i^H\mathbf{s}_j M_{r_i,r_j} \end{bmatrix} \tag{81}$$

where

$$M_{\theta_i,\theta_j} = \sum_{\ell=-1}^{L-2}\sum_{m=1}^{3}\left(\frac{\partial q_{\ell,i}}{\partial \theta_i}e_{\ell,m,i} + q_{\ell,i}\frac{\partial e_{\ell,m,i}}{\partial \theta_i}\right)^*\left(\frac{\partial q_{\ell,j}}{\partial \theta_j}e_{\ell,m,j} + q_{\ell,j}\frac{\partial e_{\ell,m,j}}{\partial \theta_j}\right) \tag{82}$$

$$M_{\theta_i,\gamma_j} = \sum_{\ell=-1}^{L-2}\sum_{m=1}^{3}\left(\frac{\partial q_{\ell,i}}{\partial \theta_i}e_{\ell,m,i} + q_{\ell,i}\frac{\partial e_{\ell,m,i}}{\partial \theta_i}\right)^*\left(q_{\ell,j}\frac{\partial e_{\ell,m,j}}{\partial \gamma_j}\right) \tag{83}$$

$\vdots$

Since for $f_i \neq f_j$, $\mathbf{s}_i^H \mathbf{s}_j \ll N$, the elements in (78) are of the order $O(N)$, whereas the elements in (81) are of the order $O(1)$. Defining a 4×4 normalizing matrix $\mathbf{D}=N^{1/2}\mathbf{I}_4$, the elements in matrices $\mathbf{D}^{-1}\mathbf{J}_{i,j}\mathbf{D}^{-1}, \forall i=j$ would be of the order $O(1)$, whereas the elements in matrices $\mathbf{D}^{-1}\mathbf{J}_{i,j}\mathbf{D}^{-1}, \forall i\neq j$ would be of the order $O(1/N)$. Therefore, for large N, the matrix $(\mathbf{I}_K \otimes \mathbf{D}^{-1})\mathbf{J}(\boldsymbol{\theta})(\mathbf{I}_K \otimes \mathbf{D}^{-1})$ would become asymptotically block diagonal. In other words, the CRBs for the parameters $(\theta_k,\gamma_k,\eta_k,r_k)$ are approximately equal to the inverse of the kth diagonal block $\mathbf{J}_{k,k}$.

Using symbolic programming by MATLAB and Mathematica, we have the following:

$$M_{\theta_k,\gamma_k}=M_{\gamma_k,\theta_k}=M_{\gamma_k,\eta_k}=M_{\eta_k,\gamma_k}=M_{\gamma_k,r_k}=M_{r_k,\gamma_k}=0 \tag{84}$$

Computing the inverse of $\mathbf{J}_{k,k}$, the following expressions for the CRBs are obtained:

$$\text{CRB}\ (\theta_k)=\frac{\sigma^2}{2N}\frac{M_{\eta_k,\eta_k}M_{r_k,r_k}-M_{\eta_k,r_k}M_{r_k,\eta_k}}{M_1-M_2-M_3+M_4+M_5-M_6} \tag{85}$$

$$\text{CRB}\ (\gamma_k)=\frac{\sigma^2}{2NM_{\gamma_k,\gamma_k}} \tag{86}$$

$$\text{CRB}\ (\eta_k)=\frac{\sigma^2}{2N}\frac{M_{\theta_k,\theta_k}M_{r_k,r_k}-M_{\theta_k,r_k}M_{r_k,\theta_k}}{M_1-M_2-M_3+M_4+M_5-M_6} \tag{87}$$

$$\text{CRB}\ (r_k)=\frac{\sigma^2}{2N}\frac{M_{\theta_k,\theta_k}M_{\eta_k,\eta_k}-M_{\theta_k,\eta_k}M_{\eta_k,\theta_k}}{M_1-M_2-M_3+M_4+M_5-M_6} \tag{88}$$

where

$$M_1=M_{\theta_k,\theta_k}M_{\eta_k,\eta_k}M_{r_k,r_k} \tag{89}$$

$$M_2=M_{\theta_k,\theta_k}M_{\eta_k,r_k}M_{r_k,\eta_k} \tag{90}$$

$$M_3=M_{\theta_k,\eta_k}M_{\eta_k,\theta_k}M_{r_k,r_k} \tag{91}$$

$$M_4=M_{\theta_k,\eta_k}M_{\eta_k,r_k}M_{r_k,\theta_k} \tag{92}$$

$$M_5=M_{\theta_k,r_k}M_{\eta_k,\theta_k}M_{r_k,\eta_k} \tag{93}$$

$$M_6=M_{\theta_k,r_k}M_{\eta_k,\eta_k}M_{r_k,\theta_k} \tag{94}$$

References

[1] H. Krim, M. Viberg, Two decades of array signal processing research: the parametric approach, IEEE Signal Processing Magazine 13 (4) (1996) 67–94.

[2] R.O. Schmidt, Multiple emitter location and signal parameter estimation, IEEE Transactions on Antennas and Propagation 34 (March) (1986) 276–280.

[3] R. Roy, T. Kailath, ESPRIT-estimation of signal parameters via rotational invariance techniques, IEEE Transactions on Acoustics, Speech, & Signal Processing 37 (July) (1989) 984–995.

[4] J.H. Kim, I.S. Yang, K.M. Kim, Passive ranging sonar based on multibeam towed array, Proceedings of IEEE Oceans, vol. 3, 2000, pp. 1495–1499.

[5] A.L. Swindlelhurst, T. Kailath, Passive direction of arrival and range estimation for near-field sources, in: IEEE Workshop on Spectrum Estimation and Modeling Workshop, 1988, pp. 123–128.

[6] C.M. Lee, K.S. Yoon, K.K. Lee, Efficient algorithm for localising 3-D narrowband multiple sources, Proceedings of Institute of Electrical Engineers: Radar, Sonar and Navigation 148 (February) (2001) 23–26.

[7] R.C. Johnson, Antenna Engineering Handbook, third ed., McGraw-Hill, New York, 1993.

[8] J.C. Chen, R.E. Hudson, Y. Kung, Maximum likelihood source localization and unknown sensor location estimation for wideband signals in the near-field, IEEE Transactions on Signal Processing 50 (8) (2002) 1843–1854.

[9] Y.D. Huang, M. Barkat, Near-field multiple sources localization by passive sensor array, IEEE Transactions on Antennas and Propagation 39 (July) (1991) 968–975.

[10] D. Starer, A. Nehorai, Passive localization of near-field sources by path following, IEEE Transactions on Signal Processing 42 (3) (1994) 677–680.

[11] J.H. Lee, C.M. Lee, K.K. Lee, A modified path-following algorithm using a known algebraic path, IEEE Transactions on Signal Processing 47 (5) (1999) 1407–1409.

[12] A.J. Weiss, B. Friedlander, Range and bearing estimation using polynomial rooting, IEEE Journal of Oceanic Engineering 18 (2) (1993) 130–137.

[13] E. Grosicki, K. Abed-Meraim, Y. Hua, A weighted linear prediction method for near-field source localization, IEEE Transactions on Signal Processing 53 (10) (2005) 3651–3660.

[14] W. Zhi, M.Y.W. Chia, Near-field source localization via symmetric subarrays, IEEE Signal Processing Letters 14 (6) (2007) 409–412.

[15] N. Yuen, B. Friedlander, Performance analysis of higher order ESPRIT for localization of near-field sources, IEEE Transactions on Signal Processing 46 (3) (1998) 709–719.

[16] R.N. Challa, S. Shamsunder, High-order subspace based algorithms for passive localization of near-field sources, in: Proceedings of 29th Asilomar Conference on Signals, Systems, and Computers, vol. 2, Pacific Grove, CA, 1995, pp. 777–781.

[17] B.A. Obeidat, Y. Zhang, M.G. Amin, Range and DOA estimation of polarized near-field signals using fourth-order statistics, Proceedings of ICASSP' 04, vol. 2, 2004, pp. 97–100.

[18] Y. Wu, L. Ma, C. Hou, et al., Subspace-based method for joint range and DOA estimation of multiple near-field sources, Signal Processing 86 (2006) 2129–2133.

[19] Y. Wu, H.C. So, J. Li, Passive localization of near-field sources with a polarization sensitive array, IEEE Transactions on Antennas and Propagation 55 (8) (2007) 2402–2408.

[20] J. Liang, X. Zeng, B. Ji, J. Zhang, F. Zhao, A computational efficient algorithm for joint range-DOA-frequency estimation of near-field sources, Digital Signal Processing 19 (4) (2009) 596–611.

[21] J. Liang, D. Liu, Passive localization of near-field sources using cumulant, IEEE Sensors Journal 9 (8) (2009) 953–960.

[22] M.D. Zoltowski, K.T. Wong, ESPRIT-based 2-D direction finding with a sparse uniform array of electromagnetic vector sensors, IEEE Transactions on Signal Processing 48 (8) (2000) 2195–2204.

[23] K.T. Wong, M.D. Zoltowski, Extended-aperture underwater acoustic multi-source azimuth/elevation direction-finding using uniformly but sparsely spaced vector-hydrophones, IEEE Journal of Oceanic Engineering 22 (4) (1997) 659–672.

[24] K.T. Wong, M.D. Zoltowski, Direction-finding with sparse rectangular dual-size spatial invariance array, IEEE Transactions on Aerospace and Electronic Systems 34 (4) (1998) 1320–1335.

[25] J. He, Z. Liu, Extended aperture 2-D direction finding with a two-parallel-shape-array using propagator method, IEEE Antennas and Wireless Propagation Letters 8 (2009) 323–327.

[26] P. Chevalier, A. Ferreol, On the virtual array concept for the fourth-order direction finding problem, IEEE Transactions on Signal Processing 47 (9) (1999) 2592–2595.

[27] P. Chevalier, L. Albera, A. Ferreol, P. Comon, On the virtual array concept for higher order array processing, IEEE Transactions on Signal Processing 53 (4) (2005) 1254–1271.

[28] J. Liang, D. Liu, Passive localization of mixed near-field and far-field sources using two-stage MUSIC algorithm, IEEE Transactions on Signal Processing 58 (1) (2010) 108–120.

[29] J. Li, Direction and polarization estimation using arrays with small loops and short dipoles, IEEE Transactions on Antennas and Propagation 41 (3) (1993) 379–387.

[30] K.T. Wong, M.D. Zoltowski, Uni-vector-sensor ESPRIT for multi-source azimuth, elevation, and polarization estimation, IEEE Transactions on Antennas and Propagation 45 (10) (1997) 1467–1474.

[31] M.C. Doğan, J.M. Mendel, Applications of cumulants to array processing I. Aperture extension and array calibration, IEEE Transactions on Signal Processing 43 (5) (1995) 1200–1216.

[32] K.T. Wong, Direction finding/polarization estimation-dipole and/or loop triads, IEEE Transactions on Aerospace and Electronic Systems 37 (2) (2001) 679–684.

[33] K.C. Ho, K.C. Tan, B.T.G. Tan, Linear dependence of steering vectors associated with tripole arrays, IEEE Transactions on Signal Processing 46 (11) (1998) 1705–1711.

[34] F.L. Hitchcock, Multiple invariants and generalized rank of a P-way matrix or tensor, Journal of Mathematical Physics 7 (1) (1927) 39–79.

[35] N.D. Sidiropoulos, R. Bro, G.B. Giannakis, Parallel factor analysis in sensor array processing, IEEE Transactions on Signal Processing 48 (8) (2000) 2377–2388.
[36] N.D. Sidiropoulos, G.B. Giannakis, R. Bro, Blind PARAFAC receivers for DS-CDMA systems, IEEE Transactions on Signal Processing 48 (3) (2000) 810–823.
[37] J.B. Kruskal, Three-way arrays: rank and uniqueness of trilinear decompositions, with application to arithmetic complexity and statistics, Linear Algebra and its Applications 18 (1977) 95–138.
[38] Y. Rong, S.A. Vorobyov, A.B. Gershman, N.D. Sidiropoulos, Blind spatial signature estimation via time-varying user power loading and parallel factor analysis, IEEE Transactions on Signal Processing 53 (5) (2005) 1697–1710.
[39] B. Afsari, Sensitivity analysis for the problem of matrix joint diagonalization, SIAM Journal on Matrix Analysis and Applications 30 (September) (2008) 1148–1171.
[40] N.M. Faber, R. Bro, K. Hopke, Recent developments in CANDECOMP/PARAFAC algorithms: a critical review, Chemometrics and Intelligent Laboratory Systems 65 (1) (2003) 119–137.
[41] G. Tomasi, R. Bro, A comparison of algorithms for fitting the PARAFAC model, Computational Statistics & Data Analysis 50 (7) (2006) 1700–1734.
[42] C.E. R Fernandes, G. Favier, J.C. Mota, Blind channel identification algorithms based on the Parafac decomposition of cumulant tensors: the single and multiuser cases, Signal Processing 88 (2008) 1382–1401.
[43] J.F. Cardoso, Super-symmetric decomposition of the fourth-order cumulant tensor. Blind identification of more sources than sensors, in: 1991 IEEE International Conference on Acoustics Speech and Signal Processing, Toronto, Canada, May 1991, pp. 3109–3112.
[44] J.F. Cardoso, A. Souloumiac, Blind beamforming for non-Gaussian signals, IEE Proceedings: F 140 (6) (1993) 362–370.
[45] P. Comon, Independent component analysis, a new concept? Signal Processing 36 (3) (1994) 287–314
[46] L.D. Lathauwer, J. Castaing, Blind identification of underdetermined mixtures by simultaneous matrix diagonalization, IEEE Transactions on Signal Processing 56 (3) (2008) 1096–1105.
[47] L.D. Lathauwer, J. Castaing, J.F. Cardoso, Fourth-order cumulant-based blind identification of underdetermined mixtures, IEEE Transactions on Signal Processing 55 (6) (2007) 2965–2973.
[48] L.D. Lathauwer, B.D. Moor, J. Vandewalle, Independent component analysis and simultaneous third-order tensor diagonalisation, IEEE Transactions on Signal Processing 49 (10) (2001) 2262–2271.
[49] E. Moreau, A generalization of joint-diagonalization criteria for source separation, IEEE Transactions on Signal Processing 49 (3) (2001) 530–541.
[50] B. Stoll, E. Moreau, A generalized ICA algorithm, IEEE Signal Processing Letters 7 (4) (2000) 90–92.
[51] A. Yeredor, Non-orthogonal joint diagonalization in the least-squares sense with application in blind source separation, IEEE Transactions on Signal Processing 50 (7) (2002) 1545–1553.
[52] J.F. Cardoso, A. Souloumiac, Jacobi angles for simultaneous diagonalization, SIAM Journal on Matrix Analysis and Application 17 (1) (1996) 161–164.
[53] A. Smilde, R.B.P. Geladi, Multi-way Analysis, John Wiley & Sons Ltd, England, 2004.
[54] S.M. Kay, Fundamentals of Statistical Signal Processing: Estimation Theory, Prentice-Hall, Upper Saddle River, NJ, 1993.